Examining the impact of the Great Barrier Reef on tsunami propagation using numerical simulations

Amanda C. Thran[1*], Sascha Brune[2,3], Jody M. Webster[4], Dale Dominey-Howes[5], Daniel Harris[6]

[1]Water Research Laboratory, School of Civil and Environmental Engineering, University of New South Wales, Sydney, New South Wales 2052, Australia.

[2]GFZ German Research Centre for Geosciences, Telegrafenberg, 14473 Potsdam, Germany.

[3]Institute of Geosciences, University of Potsdam, Potsdam, Germany

[4]Geocoastal Research Group, School of Geosciences, University of Sydney, Sydney, New South Wales 2050, Australia.

[5]Asia-Pacific Natural Hazards and Disaster Risk Research Group, School of Geosciences, University of Sydney, Sydney, New South Wales 2050, Australia.

[6]School of Earth and Environmental Sciences, University of Queensland, Brisbane, Queensland 4072, Australia.

*Corresponding author: m.thran@unsw.edu.au, +61 452 608 228

Author ORCID IDs:

- A. Thran: 0000-0002-0885-3126
- S. Brune: 0000-0003-4985-1810
- J. Webster: 0000-0002-0005-6448
- D. Dominey-Howes: 0000-0003-2677-2837
- D. Harris: 0000-0002-3275-323X

Declarations

Funding: A. T. was supported by the University of Sydney DBH Scholarship, and S. B. was supported through the Helmholtz Young Investigators Group CRYSTALS (VH-NG-1132).

Conflicts of interest/Competing interests: The authors have none to declare.

Availability of data and material: The bathymetry of the Great Barrier Reef region can be found here: http://eatlas.org.au/data/uuid/200aba6b-6fb6-443e-b84b-86b0bbdb53ac. The Great Barrier Reef Banks shapefile can be obtained here: https://data.gov.au/dataset/ds-ga-c00ab093-f02d-5b03-e044-00144fdd4fa6/details?q=great%20barrier%20reef%20banks. The global reef dataset can be downloaded here: www.wri.org/resources/data-sets/reefs-risk-revisited.

Code availability: The code Geowave can be downloaded here: http://www.appliedfluids.com/geowave.html. The codes NHWAVE and FUNWAVE-TVD can be downloaded from GitHub (github.com/JimKirby/NHWAVE; fengyanshi.github.io/build/html/index.html).

Abstract

Coral reefs may provide a beneficial first line of defence against tsunami hazards, though this is currently debated. Using a fully nonlinear, Boussinesq propagation model, we examine the buffering capacity of the Great Barrier Reef against tsunamis triggered by several hypothetical sources: a series of far-field, Solomon Islands earthquake sources of various magnitudes (M_w 8.0, M_w 8.5, and M_w 9.0), a submarine landslide source that has previously been documented in the offshore geological record (i.e. the Gloria Knolls Slide), and a potential future landslide source (i.e. the Noggin Block). We show that overall, the Great Barrier Reef acts as a large-scale regional buffer due to the roughness of coral cover and the complex bathymetric features (i.e. platforms, shoals, terraces, etc.) that corals construct over thousands of years. However, the buffering effect of coral cover is much stronger for tsunamis that are higher in amplitude. When coral cover is removed, the largest earthquake scenario (M_w 9.0) exhibits up to a 31% increase in offshore wave amplitude and estimated run-up. These metrics increase even more for landslide scenarios, where they tend to double. These discrepancies can be explained by the higher bed particle velocities incited by higher-amplitude waves, which leads to greater frictional dissipation at a seabed covered by coral. At a site-specific level, shoreline orientation relative to the reef platforms also determines the degree of protectiveness against both types of tsunamis, where areas situated behind broad, shallow, coral-covered platforms benefit the most. Additionally, we find that the platforms, rather than gaps in the offshore reef structure, tend to amplify wave trains through wave focussing when coral cover is removed from simulations. Our findings have implications for future tsunami hazards along the northeastern Australian coastline, particularly as the physiological stressors imposed by anthropogenic climate change further exacerbate coral die-off and reductions in ecosystem complexity. Therefore, areas that experience a protective benefit by the Great Barrier Reef's platforms could be disproportionately more vulnerable in the future.

Keywords:

coral reef, tsunami, Great Barrier Reef, submarine landslide, earthquake, numerical simulation

1. Introduction

Tsunamis threaten low-lying coastal communities around the world. Coral reef ecosystems, many of which are positioned between tsunami source regions and densely-populated shorelines (Figure 1), could provide a broad, cost-effective first line of defence for coastal zones (Ferrario et al. 2014). While field-based studies suggest that coral reefs induce efficient energy attenuation in wind waves due to their structural complexity (Sheppard et al. 2005; Ferrario et al. 2014; Gallop et al. 2014), a lack of consensus endures surrounding their protectiveness against tsunamis.

Following a similar logic, some post-inundation field surveys (Fernando et al. 2005; McAdoo et al. 2011) and modelling studies (Shao et al. 2019) have concluded that, due to their structural complexity, coral reef ecosystems impart similar drag-induced attenuation of wave energy on tsunamis. Other field-based studies (McAdoo et al. 2009; Fritz et al. 2011; Gelfenbaum et al. 2011) and modelling work (Kunkel et al. 2006; Yao et al. 2012; Roger et al. 2014) echo these conclusions, but with caveats. For instance, some authors caution that the buffering effect of the reef depends on where the reef is located relative to a coastal community or built asset (McAdoo et al. 2009; Fritz et al. 2011), and that wider reefs, preferably those with an extensive reef flat, appear to dissipate tsunami energy more effectively than narrower fringing reefs (Kunkel et al. 2006; Gelfenbaum et al. 2011; Yao et al. 2012; Roger et al. 2014). Conversely, others have proposed that coral reefs offer marginal to no protective benefit against tsunamis (Baird et al. 2005; Uslu et al. 2010). Further still, some field-based (Nott 1997; Chatenoux and Peduzzi 2005, 2007; Fritz et al. 2011) and modelling work (Roeber et al. 2010; Gelfenbaum et al. 2011; Yao et al. 2012; Ford et al. 2014) suggest that reefs can actually exacerbate damage along neighbouring coastlines. While there is near-universal consensus that inter-reef passages (or “gaps/openings” between reefs) can amplify tsunami waves, some argue that these amplification effects, along with other effects such as intra-lagoon resonance and increased shoaling/bore formation over shallow reef platforms, undermine any protective benefit that the presence of the reef would otherwise offer (Chatenoux and Peduzzi 2005; Liu et al. 2005; Roeber et al. 2010; Gelfenbaum et al. 2011; McAdoo et al. 2011; Ford et al. 2014; Roger et al. 2014). Despite the wide variety of methods and case studies employed to investigate this topic, the impact of coral reef ecosystems on tsunami propagation remains unclear.

Ongoing threats to the health and longevity of coral reefs under a changing climate (De'ath et al. 2012; Hughes et al. 2018) heighten these uncertainties. Decades-long field-based studies reveal declines in both coral cover and ecosystem structural complexity as critical reef-building species disappear from coral communities, leading to a progressive “flattening” of reefs (Alvarez-Filip et al. 2009; Bozec et al. 2015; Spalding and Brown 2015). It has been proposed that this decline in coral cover will reduce the protectiveness of coral reefs against other common coastal hazards, such as flooding, wind-wave exposure (both under fair weather and stormy conditions), and rising sea levels (Quataert et al. 2015; Harris et al. 2018; Storlazzi et al. 2018). The literature surrounding the impact of anthropogenically-mediated coral decline on tsunami hazards is less conclusive. However, some evidence from post-tsunami field surveys suggests that direct coral removal by means of mining and poaching intensifies tsunami wave heights and inundation extents at a local level (Fernando et al. 2005). In light of recent coral reef decline, and in the wake of recent significant tsunami events (e.g., the 2004 Indian Ocean tsunami, the 2009 South Pacific tsunamis, and the 2011 Tōhoku tsunami), a concerted effort has emerged to more rigorously assess both the present and future coastal buffering role of coral reef ecosystems against tsunamis (Chatenoux and Peduzzi 2007; Ferrario et al. 2014; Spalding et al. 2014), and this study is a contribution to that effort.

The Great Barrier Reef (GBR), the world's largest coral reef system, is an iconic feature of Australia's coastal landscape. Despite Australia's proximity to the seismically active source-regions (Dominey-Howes 2007; Davies and Griffin 2018), the manner in which tsunami behaviour is regulated by the GBR, which partitions Australia's coastline from these convergent margins, is not well understood (Webster et al. 2016). Additionally, the discovery of large (volume > 30 km^3) landslide scars and slumps on the nearby continental slope (Puga-Bernabéu et al. 2016, 2019) warrants an investigation into the GBR's ability to protect against landslide-generated tsunamis. Though believed to occur less frequently than their coseismic counterparts, landslide-generated tsunamis such as the 1998 Sissano, Papua New Guinea event (Synolakis et al. 2002) can occur suddenly within close proximity to the shoreline, causing significant localized damage and limiting opportunities for warning and swift response. This, along with the existence of possible paleo-tsunami deposits along the adjacent coastline (Nott 1997), underscores an urgency to quantify the GBR's widely-speculated role as a regional buffer from these hazards (Baba et al. 2008; Puga-Bernabéu et al. 2013a; Wei et al. 2015; Xing et al. 2015; Webster et al. 2016). However, like most coral reefs worldwide, the GBR has not escaped the consequences of anthropogenic climate change (De'ath et al. 2012; Hughes et al. 2018), and therefore, the buffering capacity of the GBR remains uncertain.

Thus far, a large portion of the debate surrounding coral reef protectiveness against tsunamis is based on findings from post-tsunami field surveys and anecdotal eye-witness accounts (Baird et al. 2005; Fernando et al. 2005; Liu et al. 2005). However, the degree of a coral reef's influence cannot be quantified solely from these field-based techniques. As many others have highlighted (Chatenoux and Peduzzi 2005; Kunkel et al. 2006; McAdoo et al. 2009; Uslu et al. 2010; Roger et al. 2014; Dilmen et al. 2018), several confounding factors can influence tsunami run-up, such as the extent of coral cover, the nature and proximity of the tsunami triggering source, and site-specific variability in coastal bathymetry and topography. Therefore, following a tsunami event, it is difficult to retrospectively ascertain the impact of coral reefs in isolation from these other site-specific factors. Numerical simulations can provide additional insights into tsunami behaviour (e.g., Kunkel et al. 2006), where experiments can be designed to systematically test the impact of coral cover and reef platform bathymetry on tsunami attenuation while keeping all other parameters, initial conditions, and boundary conditions constant (e.g., Kunkel et al. 2006). Previous studies have aimed to assess the overall impact of the GBR on tsunami propagation using numerical simulations (Baba et al. 2008; Wei et al. 2015; Xing et al. 2015; Webster et al. 2016). However, they do not account for smaller-scale structural complexity introduced by coral cover on reef platforms, and they only consider one type of tsunami source at a time.

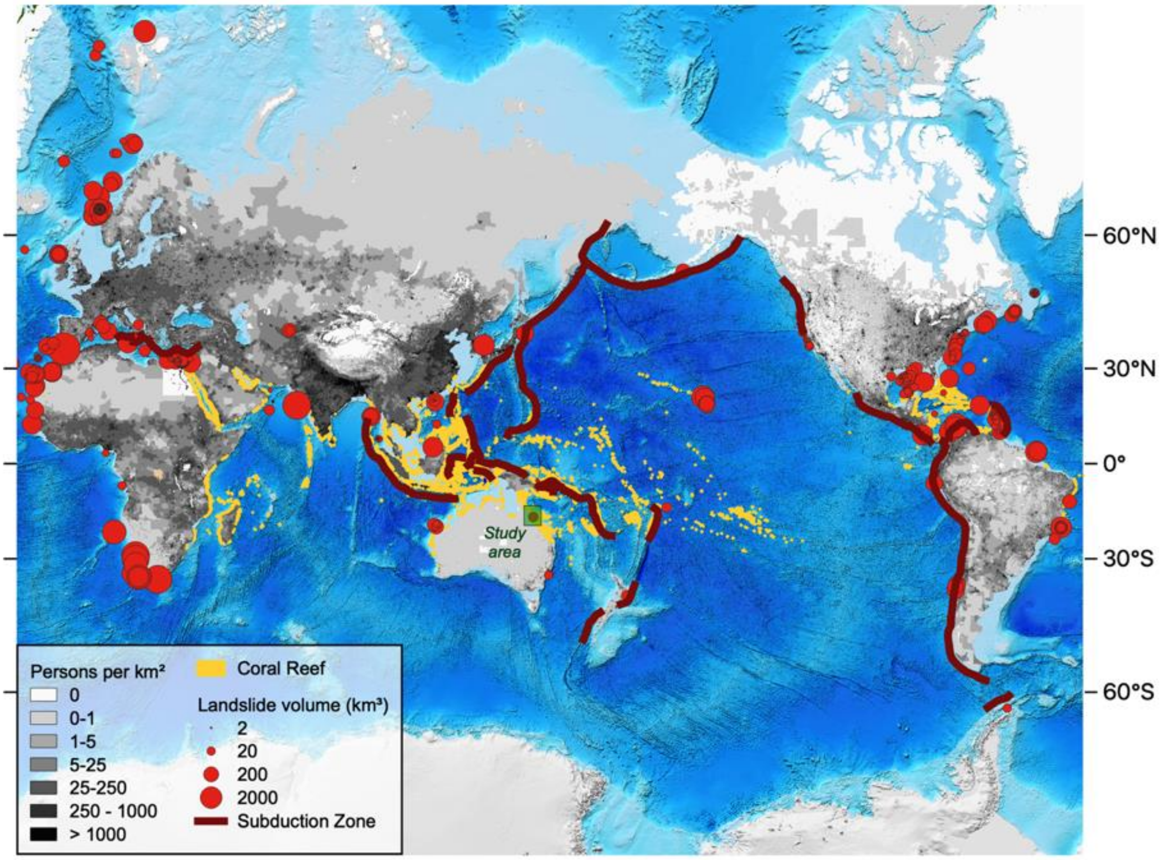

Figure 1. Global distribution of shallow-water coral reefs (Burke et al. 2011) and their proximity to tsunamigenic sources, including large submarine landslides or landslide complexes (>1 km^3; see Online Resource 1 for table of landslide events) and submarine convergent plate boundaries that constitute source-zones of major tsunamigenic earthquakes. Landslides are plotted as red circles sized proportionally to the natural log of a given landslide's volume. This compilation is based on several reviews (Hampton et al. 1996; Elverhøi et al. 2002; Owen et al. 2007; Lee 2009; Urlaub et al. 2013; Harbitz et al. 2014; Papadopoulos et al. 2014; Moscardelli and Wood 2016), where landslides with estimated volumes of 1 km^3 were excluded. All original references documenting each of the plotted slides are provided in the reference list of this study. Landmasses are overlaid with gridded UN-adjusted population density for 2020 (CIESIN 2018), with ETOPO1 as the base map (Amante and Eakins 2009).

Using numerical modelling, we evaluate the GBR's ability to shield the northeastern Australian coastline from a range of hypothetical, though plausible tsunami sources. Firstly, we consider a Solomon Islands earthquake source over various magnitudes (M_w 8.0, M_w 8.5, and M_w 9.0). Additionally, we consider two near-field landslide tsunami sources: 1) the largest documented submarine landslide event on the GBR margin (i.e. the Gloria Knolls landslide complex; Puga-Bernabéu et al. 2016), and 2) a potential collapse of a feature on the upper continental slope known as the Noggin Block (Puga-Bernabéu et al. 2013a).

In the first of a series of tsunami propagation model runs, for each tsunami source, we numerically simulate the tsunamis assuming healthy coral cover conditions (i.e. "coral-covered platforms" scenarios), where reef platforms are prescribed high roughness to reflect their structural complexity (Nelson 1996). Then, we simulate the tsunamis with smoothed reef platforms (i.e. "smooth platforms" scenarios), where we isolate the impact of live coral cover on wave attenuation (Sheppard et al. 2005). Following the methods of Baba et al. (2008), we further sequester the region's bathymetric complexity by completely excising the reef platforms from the shelf and simulating tsunami propagation with altered bathymetry (i.e. "no reef platforms" scenarios), allowing us to assess the platform-scale buffering capacity of the entire reef structure. We further test the impact of tidal phase on the buffering capacity of the GBR. We then draw upon these findings to consider the broader implications regarding present and future coral reef defence to densely inhabited, low-lying coastal areas.

2. Study area

2.1. Regional Setting

The central northeastern Australian margin is a passive margin characterised by a relatively broad (~60 km) continental shelf (Figure 2). The spring tidal range varies from north to south, but the region is generally meso- to macro-tidal (Andrews and Bode 1988). Several environmental factors favour coral reef growth on the mid- to outer-continental shelf, including the region's tropical climate, shallow seas, far proximity from terrestrial run-off, and nutrient-poor oceanographic conditions. Over hundreds of thousands of years of eustatic sea level fluctuations, these coral reef ecosystems have constructed large (up to ~300 km^2) submerged and semi-submerged carbonate platforms, pinnacles, and terraces, which comprise the offshore reef structure (Hopley et al. 2007; Hinestrosa et al. 2016). This reef structure, which underlies the modern generation of living coral cover, extends roughly 2,300 km along the mid- to outer shelf (Hopley et al. 2007). On the central margin, broad, arcuate patch reef platforms are separated by relatively wide (up to ~10 km) inter-reef passages, or "gaps" (Figure 3). While these passages are wide enough to allow some wind waves to propagate through to the inner shelf, much of the energy transferred by wind waves is attenuated atop the reef platforms (Young 1989; Gallop et al. 2014).

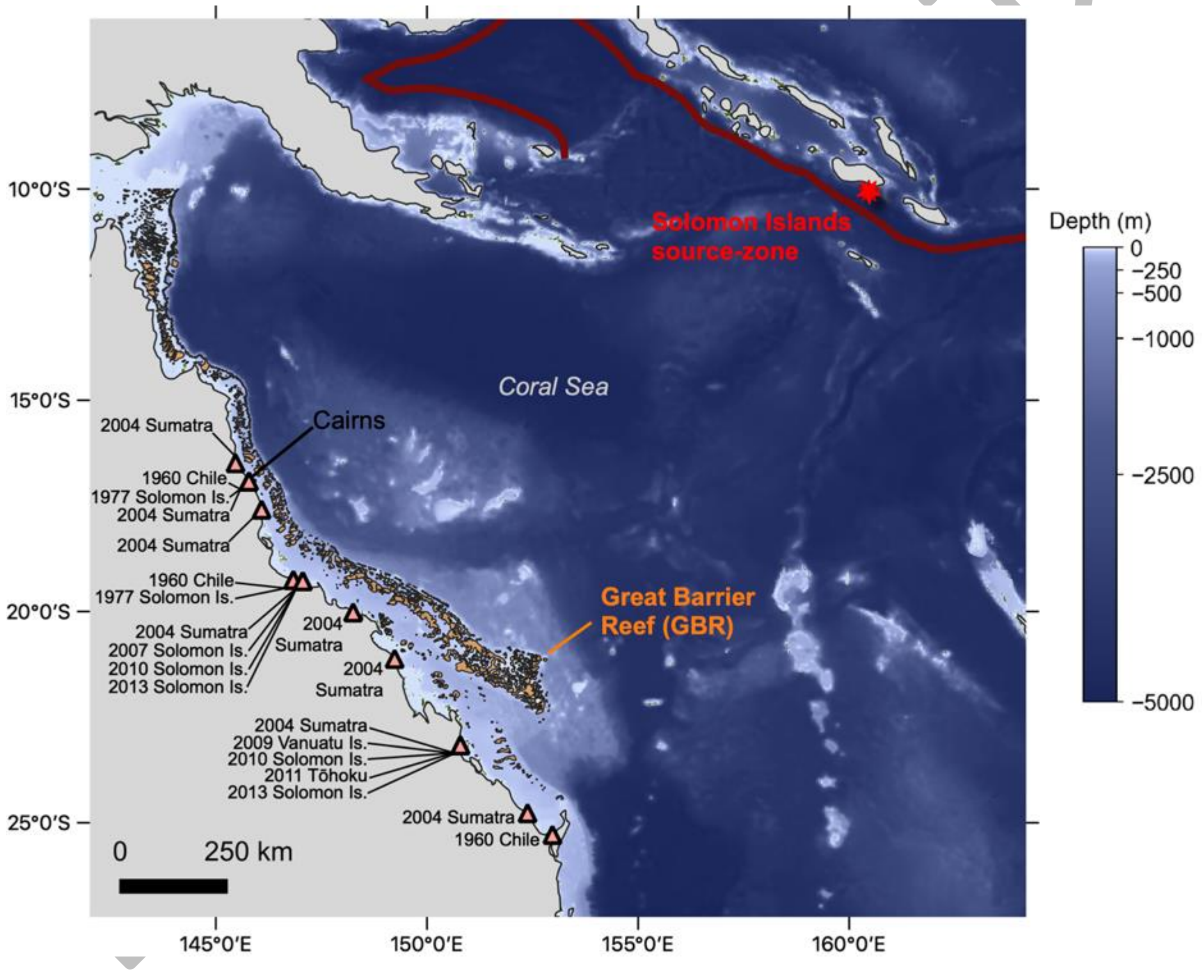

Figure 2. Regional view of the Solomon Islands source-zone, the Coral Sea, and the northeastern Australian margin, which includes the GBR (orange). Also plotted are the locations along the Australian coastline where historical tsunamis that exceeded maximum water heights of 10 cm have been observed using tide gauges (triangles; NGDC/WDS 2020). The red line indicates the subduction zones that traverse the Solomon Islands source zone.

2.2. Historical and pre-historic tsunami record

Historically, northeastern Australia has been affected by tsunamis originating from multiple regions contained within the Pacific Ring of Fire (e.g. Chile, Tonga, and more recently, Sumatra and Japan; see Figure 2). Notably, a large proportion of these historical tsunami events were triggered within subduction zones in the Solomon Islands region, which lies to the northeast of Australia across the Coral Sea (Dominey-Howes 2007; Australian Bureau of Meteorology 2020; NGDC/WDS 2020). A nationwide, probabilistic tsunami hazard assessment revealed that the Solomon Islands source-zone poses the greatest hazard to the northeastern Australian town of Cairns and the surrounding area (Davies and Griffin 2018). Therefore, the Solomon Islands source-zone was selected to simulate a range of hypothetical earthquake-generated tsunami events for this study. In contrast, the prehistoric tsunami record in northeastern Australia is much more sparse (Dominey-Howes 2007). Nonetheless, previous work has described boulder deposits that were speculated to have been emplaced by tsunami waves (Nott 1997; Figure 3).

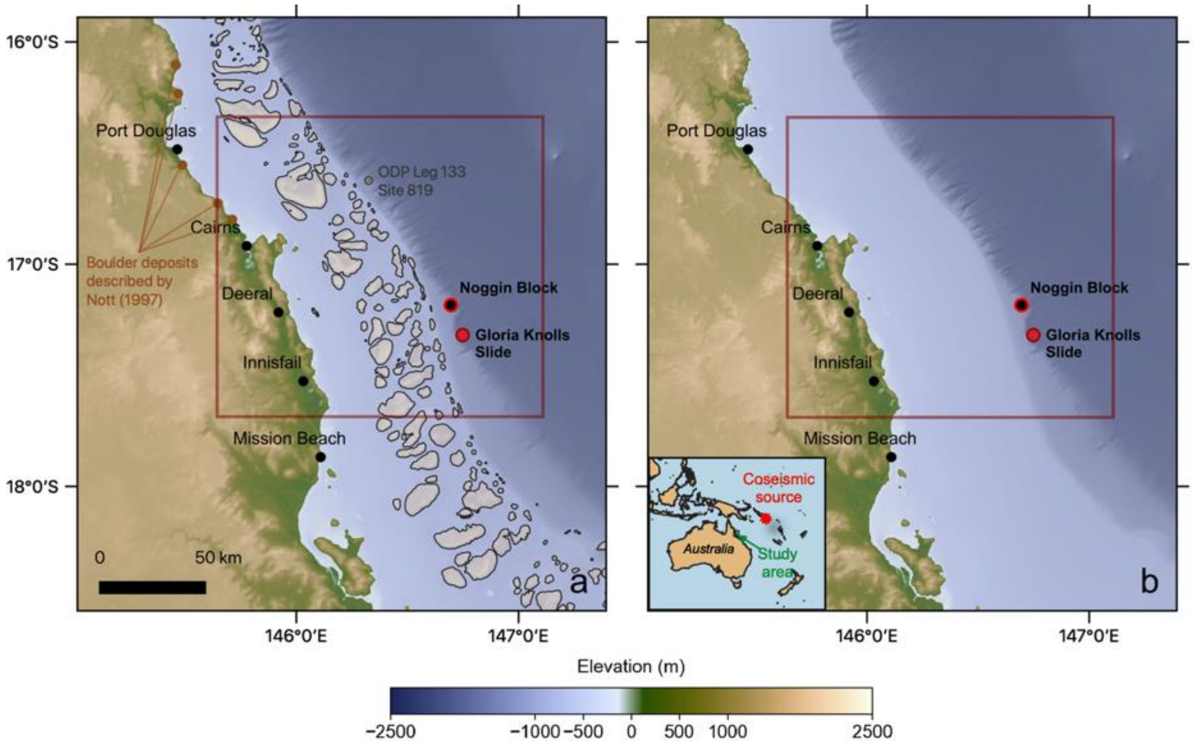

Figure 3. a) Bathymetry used in the “coral-covered platforms” and “smooth platforms” simulations. b) Bathymetry used in the “no reef platforms” simulations. Also shown are the Gloria Knolls Slide, Noggin Block, ODP Leg 133 Site 819, the locations of the boulder deposits described by Nott (1997) and the location of the hypothetical Solomon Islands coseismic sources.

2.3. Submarine landslides and areas of potential future collapse

Since the collection of high-resolution multibeam bathymetry in 2007 (Webster et al. 2008), a wide variety of submarine landslides have been described on the shelf-edge, upper, mid, and lower-slope (Puga-Bernabéu et al. 2016, 2019; Webster et al. 2016). These slides exhibit a range of different sizes and morphologies (e.g. rotational slumps, translational slides, shovel slides, carbonate terrace collapses, etc.). While they are distributed along the entirety of the margin, landslides are more commonly found on the north and central sections of the margin, where the continental slope gradient is moderate to high (4-10°, Puga-Bernabéu et al. 2011, 2013b).

The present study focuses on two notable features on the central GBR margin. The first is the Gloria Knolls landslide complex (Puga-Bernabéu et al. 2016), which is the largest among the documented submarine landslide cases on the northeastern Australian margin (total estimated volume ≈ 32 km^2). The entire complex is believed to have failed in multiple phases, with the estimated age of the first event pre-dating 300 ka (Puga-Bernabéu et al. 2016). Debris from the slide is visible in both sub-bottom profiles and in bathymetry, where the debris field extends ~20 km from the slide scarp. Roughly 8 km northwest of the Gloria Knolls slide complex lies the Noggin Block, a 4.9 x 3.5 km upper-slope feature that was previously identified as a potential area of future collapse (Puga-Bernabéu et al. 2013a). Pockmarks and adjacent landslide scars have also been described around the block (Puga-Bernabéu et al. 2013a). Slope stability modelling indicates that while the block is presently stable, seismic loading could potentially trigger a future failure (Puga-Bernabéu et al. 2013a).

We should note that it lies beyond the scope of this work to include a detailed catalogue, and thus a detailed hazard assessment, of landslide tsunami risk on this margin. A complete catalogue of all submarine landslides on the GBR margin is currently the subject of future work (Puga-Bernabéu et al., in prep).

3. Methods

3.1. Tsunami generation

3.1.1. Earthquake sources

To simulate tsunami generation by an earthquake source, the code Geowave (Watts et al. 2003) was used to produce the initial ocean free surface deformation for the hypothetical M_w 8.0, 8.5, and 9.0 coseismic events in the Solomon Islands source-zone. Tsunami generation is specifically handled in the TOPICS module of Geowave (Watts et al. 2003). The code incorporates the widely-implemented Okada elastic half-space formulation, which relates earthquake geometric source parameters (e.g. fault width, length, strike, dip, etc.) to the initial free surface deformation (Okada 1985). The Okada method has been shown to adequately reproduce free surface deformation for coseismic events exhibiting an abrupt, mostly vertical slip of the seafloor (Kowalik et al. 2005; Fujii et al. 2011) and specifically for past events that originated in the Solomon Islands (Baba et al. 2008). Source parameters were selected from the Enhanced Tsunami Scenario Database T2 (Greenslade et al., 2009; see Table 1), a suite of earthquake tsunami scenarios developed by the Joint Australian Tsunami Warning Centre and the Centre for Australian Weather and Climate Research. For simplicity, magnitude was altered by modifying the maximum fault slip parameter (see Table 1).

Table 1. List of input parameters used for tsunami wave generation models. Cases include the hypothetical Solomon Islands earthquake source (M_w 8.0, 8.5, and 9.0 scenarios), the Gloria Knolls Slide, and the Noggin Block potential landslide. Landslide volumes were calculated using the formulas of Enet & Grilli (2007), which are incorporated into NHWAVE.

Hypothetical Solomon Islands Earthquake Cases				**Landslide Cases**		
					Gloria Knolls Slide (worst case scenario)	**Noggin Block Potential Landslide**
M_w	8.0	8.5	9.0	**Latitude**	17°19'21.9"S	18°46’48”S
Maximum slip distance (m)	0.8	4.4	24.7	**Longitude**	146°45'07.4"E	148°12'01”E
Centroid latitude	9°50'13.2"S			**Length *b* (m)**	3947	4900
Centroid longitude	160°37'55.2"E			**Width *w* (m)**	19200	3500
Strike (°)	300			**Maximum thickness *T* (m)**	288	150
Dip (°)	30			**Slide volume (km^3)**	6.51	0.767
Slip rake (°)	90			**Initial submergence depth *d (m)***	420	600
Fault length (km)	400			**Mean slope *θ* (°)**	18.6	5.00
Fault centroid depth (km)	10			**Slide density (kg/m^3)**	2000	2000
Fault width perpendicular to strike (km)	80			**Slide terminal velocity (m/s)**	25.0	25.0
Shear modulus (Pa)	$4.5 \cdot 10^{10}$			**Initial acceleration a_o (m/s^2)**	0.966	0.280

3.1.2. Submarine landslide sources

To simulate tsunami generation by the Gloria Knolls Slide and the potential collapse of the Noggin Block, we used NHWAVE (Ma et al. 2013), a non-hydrostatic wave model that has been successfully validated in laboratory settings (Enet and Grilli 2007; Tehranirad et al. 2012) and has been used for several case studies of submarine mass failure-induced tsunamis (Tappin et al. 2014; Grilli et al. 2015; Li et al. 2015; Schnyder et al. 2016). The code numerically approximates the solutions to non-hydrostatic Navier-Stokes equations for incompressible flow in three dimensions, implementing a terrain-following (i.e. sigma-layered) vertical coordinate system. For simplicity and computational efficiency, a 3-dimensional, rigid, translational failure was assumed for both cases, where the bottom boundary condition is dictated by a time-varying change in depth imparted by an approximately Gaussian-shaped slide.

NHWAVE requires approximate landslide dimensions (i.e., length, width, thickness) to construct the Gaussian-shaped slide that generates the initial tsunami. For both landslide cases, these dimensions were determined in previous work (Puga-Bernabéu et al. 2013a, 2016, 2019), and were thus adopted here (see Table 1). For the Gloria Knolls Slide, slide dimensions were determined using bathymetry data containing the slide scar (Puga-Bernabéu et al. 2016, 2019). The slide is believed to have failed sequentially in multiple phases, forming what is known as a larger “slide complex”. Here, we modelled what was determined to be the worst-case scenario of these failure phases (i.e., “Event 2, Worst-Case Scenario”, see Puga-Bernabéu et al., 2019). This case was selected to represent one of the most severe submarine landslide cases for this region, as the Gloria Knolls Slide is, thus far, the largest documented slide complex (total volume ≈ 32 km^3) on the northeastern Australian margin (Puga-Bernabéu, in prep). For the Noggin Block, the initial dimensions were determined from a rigorous, modelling-based slope stability analysis conducted for the block (Puga-Bernabéu et al. 2013a). This feature is comparatively small; the estimated slide volume is ~0.77 km^3 (using the volume formulas of Enet & Grilli, 2007). However, the block is relatively shallow, resting on the upper slope (~ 400 m). An additional sensitivity analysis was conducted to test the impact of failure depth on the initial tsunami wave height (see Section 4.2).

For both landslide cases, kinematic parameter a_0 was determined using the semi-empirical formulations of Enet and Grilli (2007), and the peak slide velocity was prescribed a value of 25 m/s. This peak velocity is of similar magnitude to those recorded by submarine cable breaks during the Grand Banks Event (i.e., 20-25 m/s; Fine et al., 2005). A landslide density of 2000 kg/m^3 was informed by sediment core measurements obtained by Ocean Drilling Program (ODP) Leg 133 Site 819, which was drilled ~70 km north of the Noggin Block and the Gloria Knolls Slide (Davies et al. 1991). Each simulation was run for a landslide failure duration of 3 minutes at 100 m resolution horizontally and at 5 sigma layers vertically.

3.2. Tsunami propagation

The resulting ocean free surface elevations, as well as the depth-averaged zonal and meridional velocities, were smoothed and re-interpolated from the tsunami generation model outputs to set the initial conditions for the wave propagation model. Tsunami propagation was modelled using FUNWAVE-TVD (Shi et al. 2012), a widely-used, fully nonlinear Boussinesq tsunami propagation code that has been validated against NOAA's National Tsunami Mitigation Program benchmark requirements (NTHMP, 2012). The model captures wave behaviours such as shoaling, dissipation via bottom friction and wave breaking, and frequency dispersion (Shi et al. 2012).

For the earthquake scenarios, tsunami propagation was simulated across the Coral Sea using a 1 arcminute ETOPO1 grid (Amante and Eakins 2009). Smaller nested grids of 200 x 200 m resolution were used to resolve the earthquake-generated waves upon arrival to the continental shelf. These grids were generated from a 100 m resolution bathymetric dataset spanning the entire northeastern Australian margin, including the GBR (i.e. “3DGBR”, Beaman, 2010; see Figure 3a). Waves were introduced into the smaller nested grids via a one-way coupling scheme. Near-field landslide scenarios were also simulated with grids generated from the 3DGBR bathymetric dataset. Bathymetry for all cases was smoothed using a Gaussian filter to prevent numerical instability incited by steep bathymetric slopes.

The spatial resolution of the model domains was carefully selected using a range of sensitivity analyses (see Online Resource 2). For the earthquake scenarios, a 200 x 200 m grid is deemed sufficient to resolve interactions between the propagating waves and the seafloor. The Gloria Knolls Slide and the Noggin Block potential failure necessitated finer resolution grids to adequately resolve shoaling and scattering processes (100 m and 50 m resolution, respectively).

It is important to note here that although Geowave also has the ability to simulate tsunami generation and propagation by both coseismic slip and landslide sources, we opted to use updated models that more explicitly resolve processes involved in landslide tsunami generation (i.e. the non-hydrostatic formulations of NHWAVE) and more accurately represent frequency dispersion of propagating gravity waves (i.e. the improved fully-nonlinear, Boussinesq formulations of FUNWAVE-TVD). Dispersive effects become more critical to simulate for far-field and landslide tsunami sources (Tehranirad et al. 2015).

3.3. Run-up estimation

In the absence of the nearshore high-resolution bathymetric and topographic data (<50 m) required to accurately resolve onshore tsunami inundation, final estimated run-up distributions were calculated using virtual tide gauges placed along the shoreline in ~25 m water depth *d* using the following equation:

$$R = A(d)^{\frac{4}{5}} \cdot d^{\frac{1}{5}} \qquad \text{(Eq.1)}$$

where *R* is the estimated run-up and *A*(*d*) is the maximum wave amplitude at a virtual gauge location at depth *d*. This formula is based on the conservation of wave energy flux and applies to both breaking and non-breaking waves (Ward and Asphaug 2003).

3.4. Testing the impact of the GBR on tsunami propagation

A major objective of this study is to test whether the structural complexity of the GBR plays a role in attenuating tsunami wave energy. The GBR exhibits structural complexity at two predominant spatial scales. Firstly, due to the morphological diversity of individual species, coral cover is structurally complex on the meter to sub-meter scale (Nelson 1996; Graham and Nash 2013). We hereafter refer to the structural complexity of coral cover as “ecosystem-scale” complexity. In a modelling context, this “ecosystem-scale” complexity cannot be resolved in the computational domain and must be parameterized (see Section 3.4.1). Secondly, the GBR exhibits structural complexity at the >1 km scale. The reef structure itself is composed primarily of completely submerged or semi-submerged carbonate platforms. These features create complex positive relief on the submerged continental shelf, and much of this relief (aside from smaller, deeper pinnacles and terraces), is resolved by the 100 m-resolution 3DGBR bathymetric dataset (Beaman 2010). Thus, the reef structure can be adequately resolved in the computational domain. We hereafter refer to complexity introduced by the reef structure as "bathymetric-scale" complexity.

The following sections detail how the impact of GBR's structural complexity at both the ecosystem-scale and bathymetric-scale was tested.

3.4.1. Ecosystem-scale complexity: coral cover parameterization

In FUNWAVE-TVD, bottom shear stress τ is calculated using the standard quadratic drag law (Shi et al. 2016):

$$\tau = \frac{1}{2}\rho C_D U^2 \qquad \text{(Eq.2)}$$

where C_D is the non-dimensional bottom friction coefficient, ρ is the density of water, and U is the particle velocity at the seabed. A variable bottom friction coefficient was established throughout the domain, where it was altered according to the presence or absence of coral cover on reef platforms. A value of C_D=0.1522 was prescribed to reef platforms to simulate coral cover (average depth of platforms ≈ 14.9 m). This value was obtained from a prior field investigation of the hydraulic roughness of coral reefs, which was conducted at John Brewer Reef, a reef platform within the GBR that lies close to the study region (Nelson, 1996; ~80 km from the computational domain). Additionally, this coefficient falls well within the range of values obtained for other reefs (Monismith et al. 2013). All other areas of the computational domain where prescribed the conventional value of C_D = 0.0025, which is representative of sand-covered seafloor (Grilli et al. 2015). This approach was used to create the "coral cover" scenarios, where the ecosystem-scale structural complexity of the GBR was taken into account in tsunami propagation simulations (Figure 3a).

To test the impact of coral cover on tsunami attenuation, the "coral cover" scenarios were then compared to "smooth platform" scenarios, where coral cover was effectively removed. In the "smooth platform" scenarios, all areas of the bottom boundary, reef platforms included, were prescribed a standard bottom friction coefficient value of $C_D = 0.0025$.

3.4.2. Bathymetric-scale complexity: testing the impact of the reef platforms

Larger-scale, bathymetric complexity is introduced by the reef structure itself, which is composed primarily of reef platforms. Testing the impact of these platforms on tsunami propagation requires artificial bathymetry, where the positive relief formed by the platforms is removed from the shelf (Figure 3b). Platforms were removed by "cookie-cutting" the bathymetry, removing areas of the mid- to outer-shelf containing the reef platforms. The bathymetry was then linearly interpolated and smoothed over the cookie-cut areas employing a Gaussian filter. This modified bathymetry was then used in the "no reef platforms" scenarios.

3.5. Testing the additional effect of tidal phase

As the central northeastern Australian margin is a meso-tidal environment, water depths over the reef platforms can vary significantly over several hours. Consequently, tidal phase has been shown to modulate the degree of wind wave attenuation (Young and Hardy 1993). To test the impact of tidal phase on tsunami propagation, two additional scenarios were configured: one where the highest spring tide (+1.75 m above MSL) and one where the lowest spring tide (-1.75 m above MSL) coincided with tsunami arrival at the GBR.

4. Results

4.1. Earthquake tsunami generation and regional propagation

For the hypothetical M_w 8.0, 8.5, and 9.0 Solomon Islands earthquake scenarios, the generation model simulates initial peak wave amplitudes of 0.32 m, 1.7 m, and 9.7 m, respectively (Figure 4). The tsunamis in each case then propagate across the Coral Sea to the outer GBR margin after an approximately 3.5 hour travel time, which is consistent with previous travel times observed for the Solomon Islands source-zone (NGDC/WDS 2020). Upon arrival to the outer Australian continental shelf within the nested domain, wave amplitudes range from ~1-2 cm for the M_w 8.0 case, ~6-10 cm for the M_w 8.5 case, and ~30-60 cm for the M_w 9.0 case.

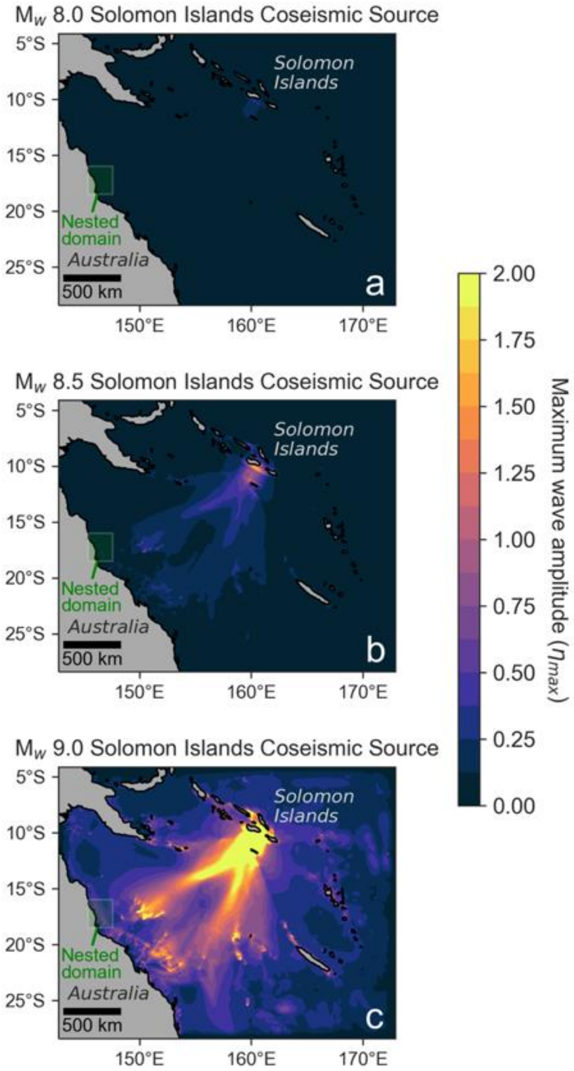

Figure 4. Maximum wave amplitudes simulated by FUNWAVE-TVD for the hypothetical M$_w$ 8.0 (a), M$_w$ 8.5 (b), M$_w$ 9.0 (c) Solomon Islands earthquake sources. Initial maximum wave amplitudes at the source are 0.32 m, 1.7 m, and 9.7 m, respectively. The simulated propagation time represented here is ~8 hours to allow waves to reach all parts of the bathymetric domain.

4.2. Landslide tsunami generation

The landslide generation model NHWAVE simulates ~18 m-high seaward-propagating wave crest and ~9 m-high landward-propagating wave crest for the Gloria Knolls Slide (Figure 5), assuming the previously-determined worst-case scenario (Puga-Bernabéu et al. 2019). For the potential collapse of the Noggin Block, the landslide generation model simulates a ~1.3 m-high seaward-propagating crest and a ~3.5 m-high landward-propagating crest (Figure 6a). Sensitivity analyses indicate that initially generated wave amplitudes are responsive to moderate changes in depth (+/- 100 m). If the block was to initially fail 100 m deeper (500 m depth), the wave amplitude of the landward-propagating crest reaches ~ 2.5 m, about 71% of its original value. On the other hand, should the block fail at a 100 m-shallower depth (300 m depth), the wave amplitude peaks at ~4.8 m, growing roughly 37%. For the subsequent simulations of tsunami propagation, the main Noggin Block scenario (failure depth = 400 m) is implemented.

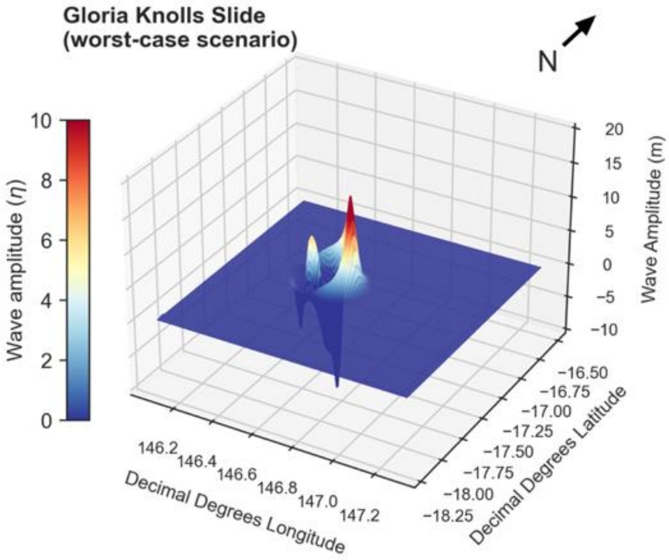

Figure 5. Instantaneous free surface elevation at t = 9 min for the Gloria Knolls landslide tsunami scenario, simulated using NHWAVE. Wave amplitude peaks at $\eta \approx 18$ m. The smaller peak is the landward-propagating wave, and it peaks at $\eta \approx 9$ m.

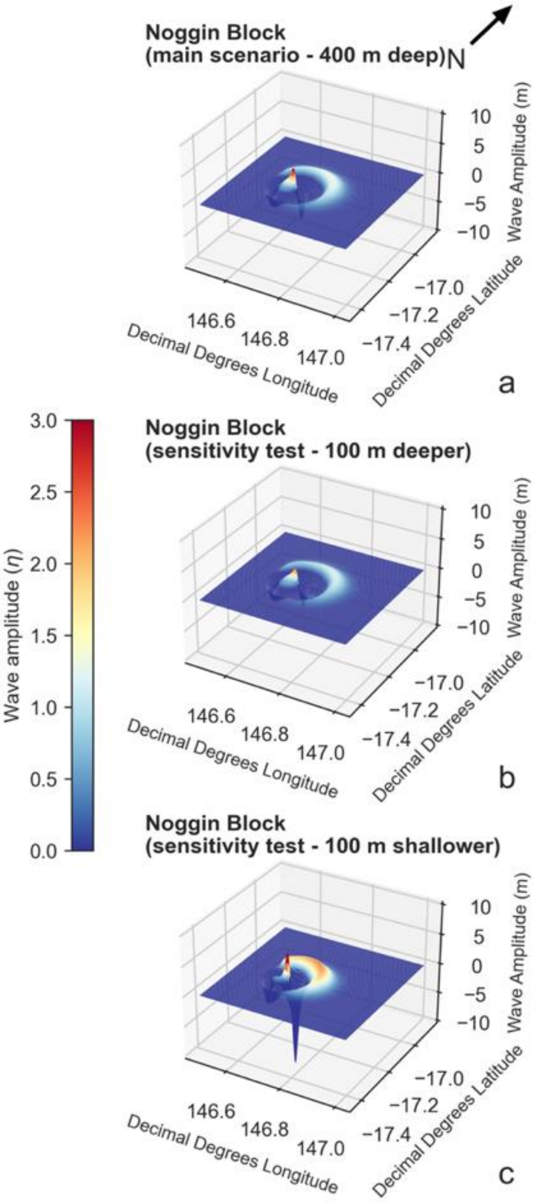

Figure 6. Instantaneous free surface elevations at t = 9 min for the potential Noggin Block collapse, simulated using NHWAVE. The main scenario (a) assumes a failure depth of ~400 m, where the peak wave amplitude for the landward-propagating crest reaches ~ 3.5 m. A sensitivity test indicates that a 100 m-deeper failure (b) would result in a substantially smaller wave crest ($\eta_{max} \approx 2.5$ m, 71% of its original value). A 100 m-shallower failure (c) would result in a larger initial wave crest ($\eta_{max} \approx 4.8$ m, 37% greater than its original value).

4.3. Nearshore earthquake tsunami propagation

Results indicate that the GBR's buffering impact on the earthquake-generated tsunami, which originates in the Solomon Islands source-zone, depends on the magnitude of the initial earthquake. Turning firstly to the hypothetical M_w 8.0 earthquake scenario (Figure 7a), maximum wave amplitudes across the domain remain under 5 cm when coral cover is present atop the reef platforms (i.e. when ecosystem-scale complexity is high), where maximum estimated run-up R_{max} reaches ~6.2 cm. When coral cover is removed (Figure 7b), maximum wave amplitudes increase marginally or remain the same, growing 2% on average along the 25 m isobath (Figure 7c). Estimated run-ups follow a similar trend ($R_{max} \approx 6.4$ cm). Finally, when reef platforms are removed from bathymetry (Figure 7c), offshore wave amplitudes increase a bit more substantially (17% on average), but still fall below ~5 cm across the domain. The maximum run-up estimate remains at a similar elevation ($R_{max} \approx 6.7$ cm, Figure 7d).

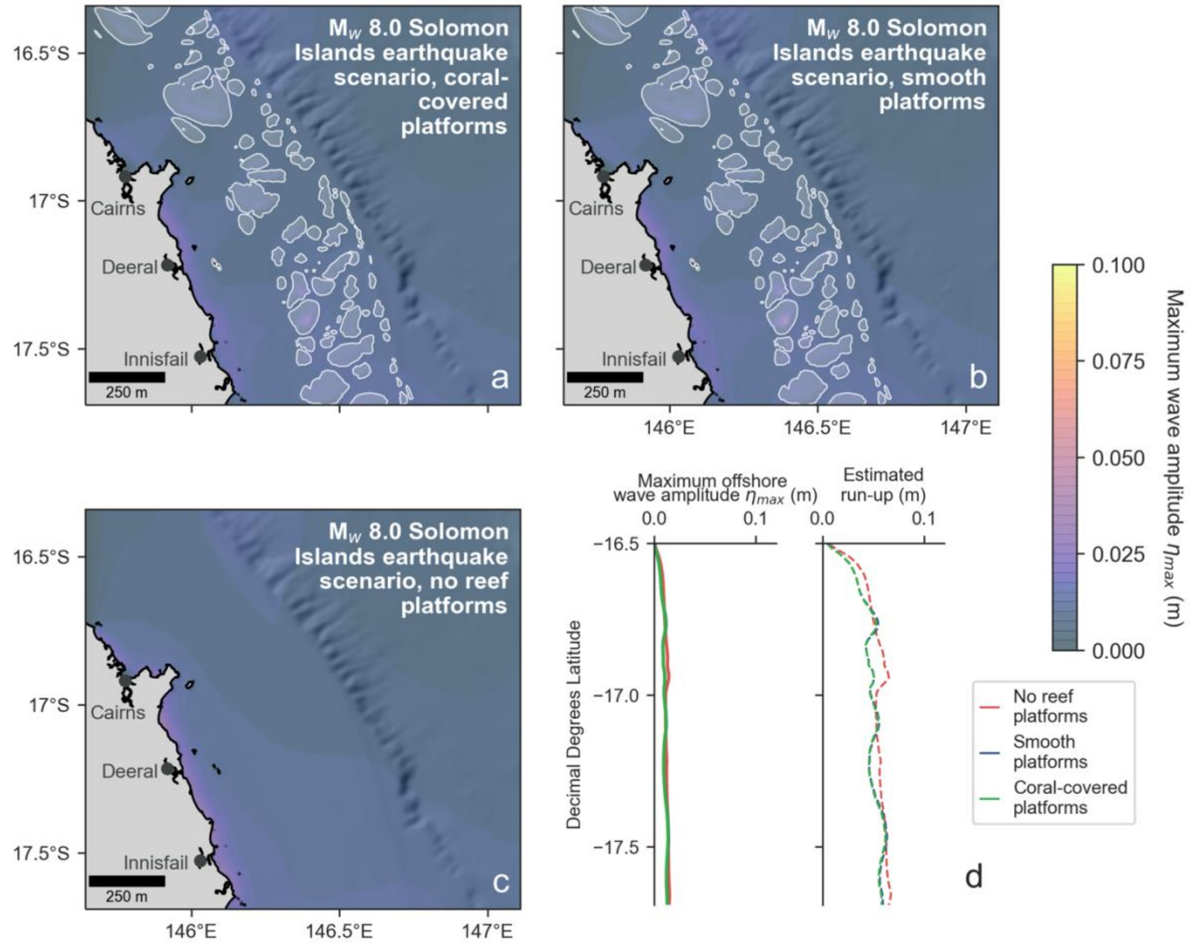

Figure 7. Maximum wave amplitude distributions for the hypothetical M_w 8.0 Solomon Islands earthquake scenario simulated with a) the modern "coral-covered platforms" (bottom friction coefficient C_D=0.1522 on platforms, shown in white) b) "smooth platforms" (C_D=0.0025), and c) "no reef platforms". d) Corresponding maximum offshore wave amplitude and estimated run-up distributions. Maximum run-up estimates are 6.2 cm

for the “coral-covered platforms” scenario, 6.4 cm for the “smooth platforms” scenario, and 6.7 cm for the “no reef platforms” scenario. Offshore wave amplitudes were interpolated along the 25 m isobath.

For the hypothetical M_w 8.5 Solomon Islands earthquake scenario, the GBR, both in terms of its ecosystem-scale and bathymetric scale complexity, appears to have slightly more impact on offshore tsunami amplitudes and estimated run-up. When coral cover is present (Figure 8a), wave amplitudes landward of the GBR range from ~5-10 cm, with an R_{max} estimate of ~26 cm. When platforms are smoothed (Figure 8b), these amplitudes grow, increasing 7% on average along the 25 m isobath. The maximum run-up estimate also increases slightly ($R_{max} \approx 28$ cm). Wave amplitudes similarly increase when reef platforms are removed (Figure 8c; 13% average increase along the 25 m isobath; $R_{max} \approx 32$ cm). Overall, the changes in the amplitude and run-up distributions are moderate for this case (Figure 8d).

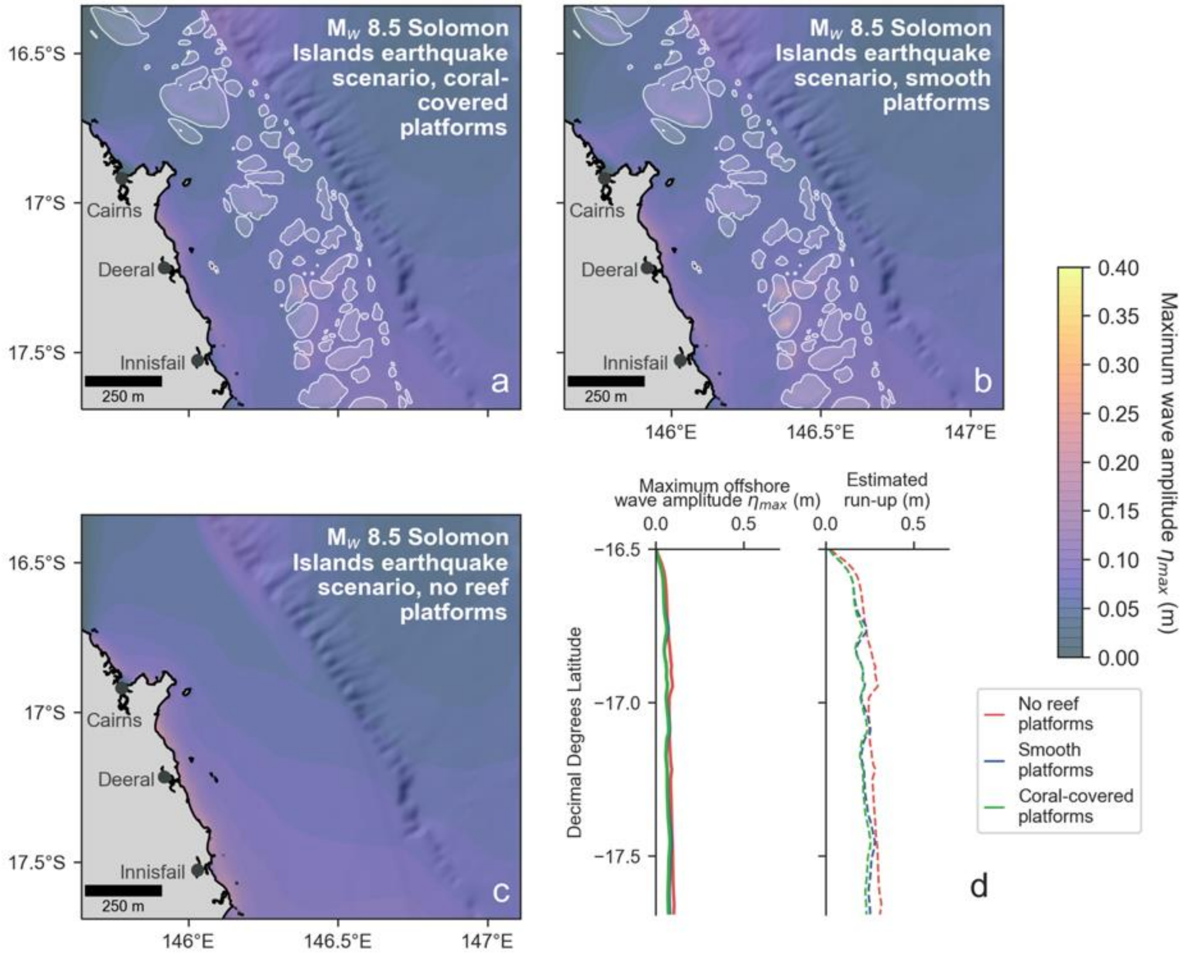

Figure 8. Maximum wave amplitude distributions for the hypothetical M_w 8.5 Solomon Islands earthquake scenario simulated with a) the modern "coral-covered platforms" (bottom friction coefficient C_D=0.1522 on platforms, shown in white) b) "smooth platforms" (C_D=0.0025), and c) "no reef platforms". d) Corresponding maximum offshore wave amplitude and estimated run-up distributions. Maximum run-up estimates are 26 cm for the "coral-covered platforms" scenario, 28 cm for the "smooth platforms" scenario, and 32 cm for the "no reef platforms" scenario. Offshore wave amplitudes were interpolated along the 25 m isobath. For animations of tsunami propagation for the "coral-covered platforms" and "no reef platforms" scenarios, see Online Resources 3 and 4.

The GBR has a much more substantial impact on the propagating tsunami when considering the hypothetical M_w 9.0 Solomon Islands earthquake source. Overall, the M_w 9.0-generated tsunami is significantly larger in amplitude than its smaller-magnitude counterparts. When coral cover is present on reef platforms, maximum offshore wave amplitudes range from about 0.2-0.4 m landward of the GBR (Figure 9a), resulting in a maximum estimated run-up of ~0.85 m. When platforms are smoothed (Figure 9b), amplitudes increase (18% on average along the 25 m isobath), particularly directly landward of broad reef platforms. Likewise, the maximum estimated run-up increases when platforms are smoothed, reaching 1 m. Finally, when reef platforms are removed from bathymetry, amplitudes increase substantially on the shelf (51% on average along the 25 m isobath), leading to a maximum estimated run-up of ~1.2 m (Figure 9d).

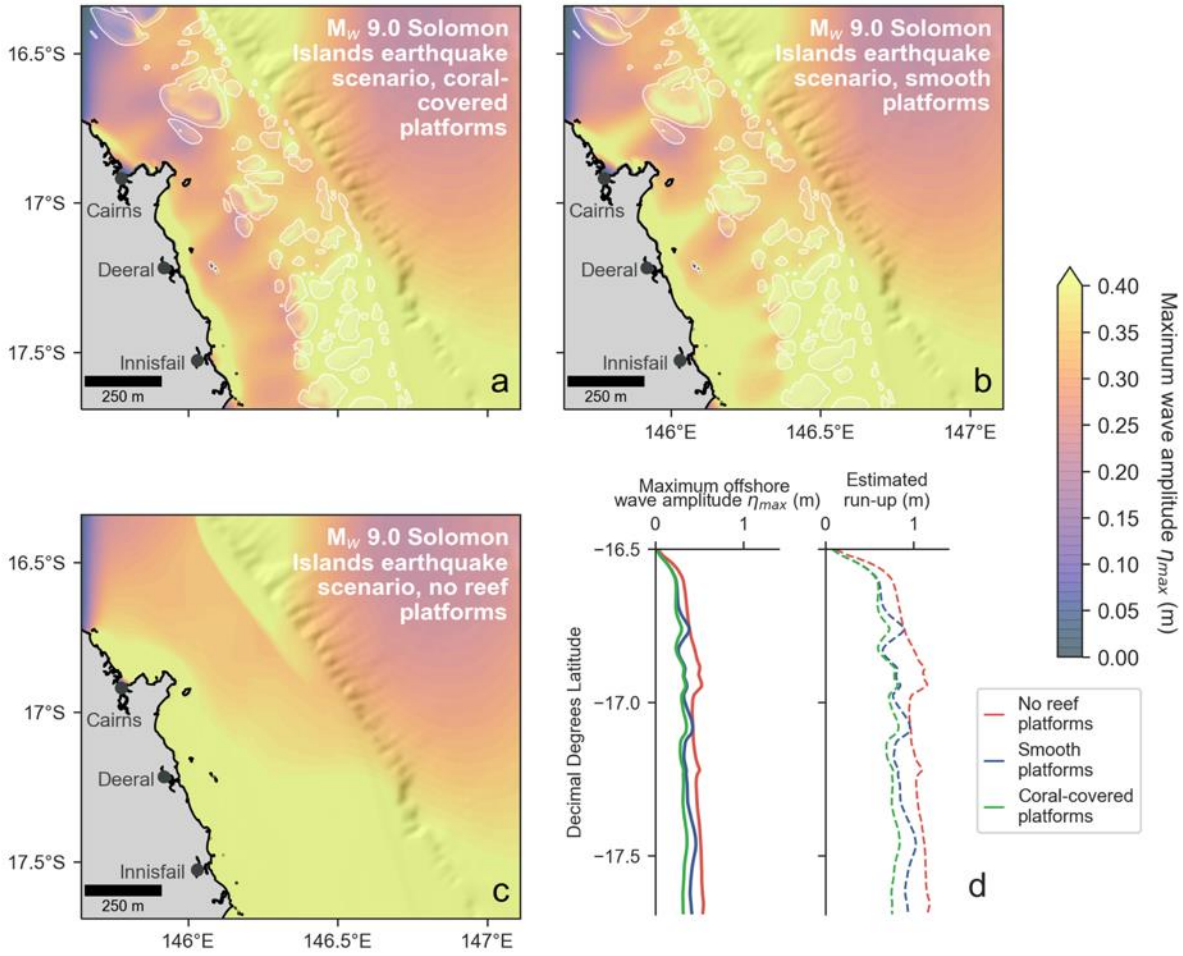

Figure 9. Maximum wave amplitude distributions for the hypothetical M_w 9.0 Solomon Islands earthquake scenario simulated with a) the modern “coral-covered platforms” (bottom friction coefficient C_D=0.1522 on platforms, shown in white) b) “smooth platforms” (C_D=0.0025), and c) “no reef platforms”. d) Corresponding maximum offshore wave amplitude and estimated run-up distributions. Maximum run-up estimates are 0.85 m for the “coral-covered platforms” scenario, 1.0 m for the “smooth platforms” scenario, and 1.2 m for the “no reef platforms” scenario. Offshore wave amplitudes were interpolated along the 25 m isobath.

Figure 10 shows the percentage increase exhibited by both offshore wave amplitude and predicted run-up when both the ecosystem-scale and bathymetric-scale complexity of the GBR is removed. This gives an indication of the relative degree to which the GBR attenuates tsunami wave energy. Firstly considering ecosystem-scale complexity isolation, when coral cover is removed, under the M_w 8.0 scenario (Figure 10a), wave amplitudes are slightly larger on a percentage-wise basis compared to when coral cover is present, ranging from 0-4% increase within the study area. For the M_w 8.5 scenario, this percentage increase heightens, ranging from 1-15%. Finally, for the largest earthquake scenario (M_w 9.0), amplitudes increase substantially, ranging from 3-31% higher compared to when coral cover is present. Percentage increases in the estimated run-up distributions follow similar patterns. Amplitude and run-up increases are highly variable alongshore, with the largest peaks occurring directly behind shelf areas with broad, shallow reef platforms. For instance, the city of Cairns (latitude ≈ 16.8°S) seems to benefit from being situated behind a wide, shallow reef platform that lies in the path of the tsunami. The overall trend indicates that the attenuating effect of coral cover increases with the magnitude of the earthquake source.

The second panel of Figure 10 reflects the very substantial combined attenuative impact of ecosystem-scale and bathymetric-scale complexity (i.e. coral cover and reef platforms). When coral cover and reef platforms are removed, wave amplitudes and run-ups increase considerably for the M_w 8.0 scenario (range: 0-48%). Notably, at a few locations, this percentage dips marginally below zero (-5% maximum), indicating that these areas would experience a *decrease* in offshore amplitudes and estimated run-ups if reef platforms were not present. Amplitude and run-up distributions follow a similar pattern, increasing overall for the M_w 8.5 (range: 7-70%), and again for the M_w 9.0 (range: 20-90%). These results reflect the significant combined attenuative impact of both coral cover and the reef platforms on the propagating tsunamis, which increases with earthquake source magnitude. We again note the immense variability of the amplitude and run-up increases alongshore for each earthquake scenario.

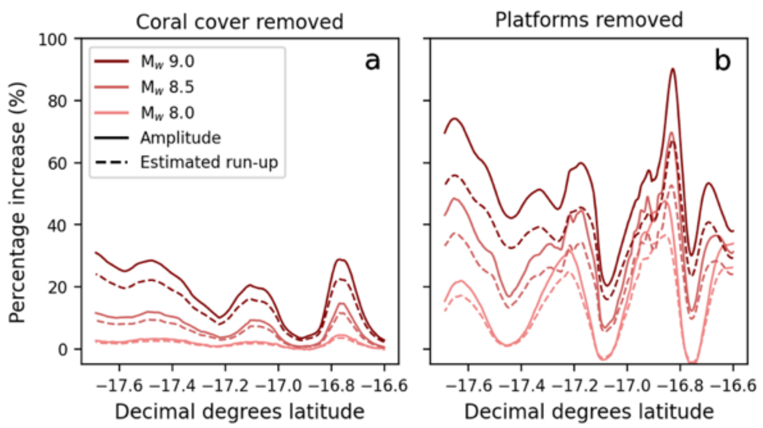

Figure 10. Percentage increases in both earthquake tsunami amplitude and estimated run-up when a) coral cover is removed and b) reef platforms are removed. Amplitudes, which were also used to calculate run-up, were extracted along the 25 m isobath.

For all cases, the first tsunami waves arrive at the coast after an approximately 4 hr travel time from the Solomon Islands source-zone. When passing over the shelf, the tsunami experiences diffraction, shoaling, and focusing. In particular, broad, moderately deep platforms tend to focus tsunami wave energy towards shore (e.g., Figure 9b). When platforms are removed, this behaviour disappears. For animations of the M_w 8.5 scenario simulated with coral cover and no reef platforms, see Online Resources 3 and 4.

4.4. Nearshore landslide tsunami propagation

Simulations indicate that the impact of ecosystem-scale and bathymetric-scale complexity on tsunami attenuation is sizeable for the landslide-generated cases considered on this margin. Turning firstly to the previously-termed “worst-case scenario” for the Gloria Knolls Slide (Puga-Bernabéu et al. 2016), when reef platforms are covered by coral, offshore amplitudes markedly decline from over ~4 m to under ~2 m landward of the platforms (Figure 11a), and maximum estimated run-up is estimated reaches up to ~2.2 m. When coral cover is removed (Figure 11b), offshore amplitudes along the 25 m isobath nearly double, increasing by a factor of ~1.9 on average. Maximum estimated run-up rises to ~3.9 m under the “smooth platforms” simulation. When reef platforms are removed (Figure 11c), offshore amplitudes more than quadruple on average (fold-change: ~4.6), when compared to the “coral-covered platforms” scenario. When platforms are absent, estimated maximum run-up increases again, reaching 4.6 m (Figure 11d). The total elapsed time between tsunami generation and the arrival of the first waves is ~1.5 hrs.

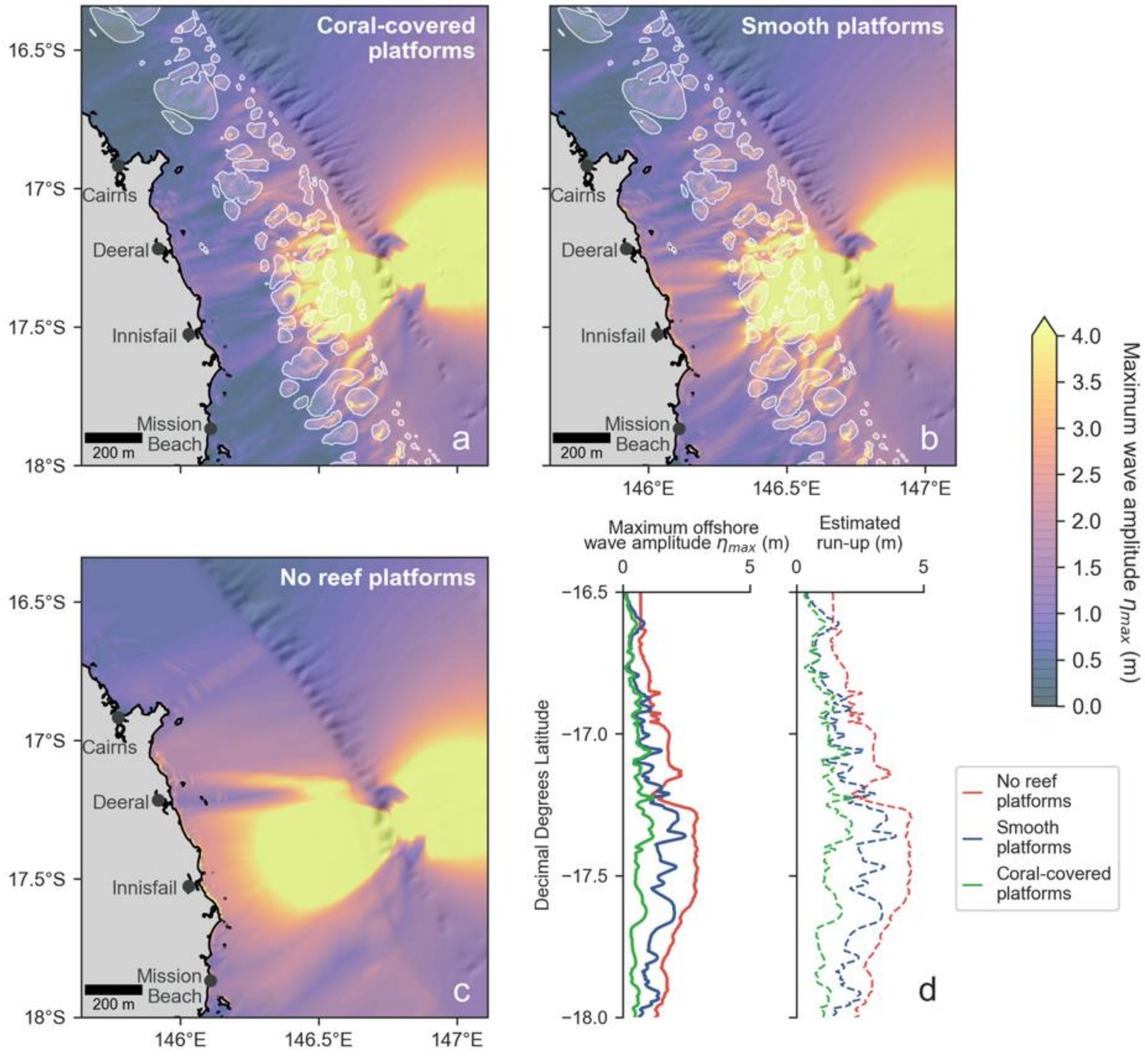

Figure 11. Maximum wave amplitude distributions for the Gloria Knolls Slide (worst-case scenario) simulated with a) the modern “coral-covered platforms” (bottom friction coefficient C_D=0.1522 on platforms, shown in white) b) “smooth platforms” (C_D=0.0025), and c) “no reef platforms”. d) Corresponding maximum offshore wave amplitude and estimated run-up distributions. Maximum run-up estimates are ~2.2 m for the “coral-covered platforms” scenario, ~3.9 m for the “smooth platforms” scenario, and ~4.6 m for the “no reef platforms” scenario. Offshore wave amplitudes were interpolated along the 25 m isobath. For animations of the “coral-covered platforms” and “no reef platforms” scenarios, see Online Resources 5 and 6.

Results for the Noggin Block potential slide are very similar to that of the Gloria Knolls Slide, though it produces a smaller tsunami (see Section 4.2). Assuming healthy reef growth (Figure 12a), offshore amplitudes remain under ~1 m, where they sharply decline upon passing over the GBR platforms. Maximum estimated run-up for this scenario is ~1.4 m. When coral cover is removed (Figure 12b), offshore amplitudes along the 25 m isobath increase by a factor of ~2 on average, with the maximum run-up rising to 1.8 m. Finally, when platforms are removed from the simulations (Figure 12c), offshore amplitudes along the 25 m isobath are, on average, 4.5 times larger than the original "coral cover" scenario. Peak estimated run-up reaches ~2.8 m under the "no reef platforms" scenario (Figure 12d). The total time between tsunami generation and the arrival of the first waves is similar to the Gloria Knolls landslide tsunami (~1.5 hrs).

Figure 10 shows the overall change in offshore wave amplitude and estimated-runup when coral cover and reef platforms are removed from simulations, this time represented in terms of fold-change rather than percentage change. For each landslide case, offshore amplitudes along the 25 m isobath, along with estimated run-ups, tend to double when coral cover is removed (Figure 10a). When platforms are removed, the amplitudes and run-ups increase significantly for each case, but more so for the Noggin Block potential slide (Figure 10b). Again, we highlight the enormous along-shore variability in amplitude and run-up change across simulations.

Landslide tsunamis across both cases exhibit common behaviours. Amplitude and run-up distributions follow a localized bell-curve due to radial damping, a standard process undergone by point-source tsunamis (Brune et al., 2010; Harbitz et al., 2006). Additionally, reef platforms greatly interfere with these comparably shorter waves as they traverse the shallow continental shelf (Harbitz et al., 2006). For animations of both the Gloria Knolls slide scenario simulated with coral-covered platforms and no reef platforms, see Online Resources 5 and 6. For the same corresponding Noggin Block landslide tsunamis, see Online Resources 7 and 8.

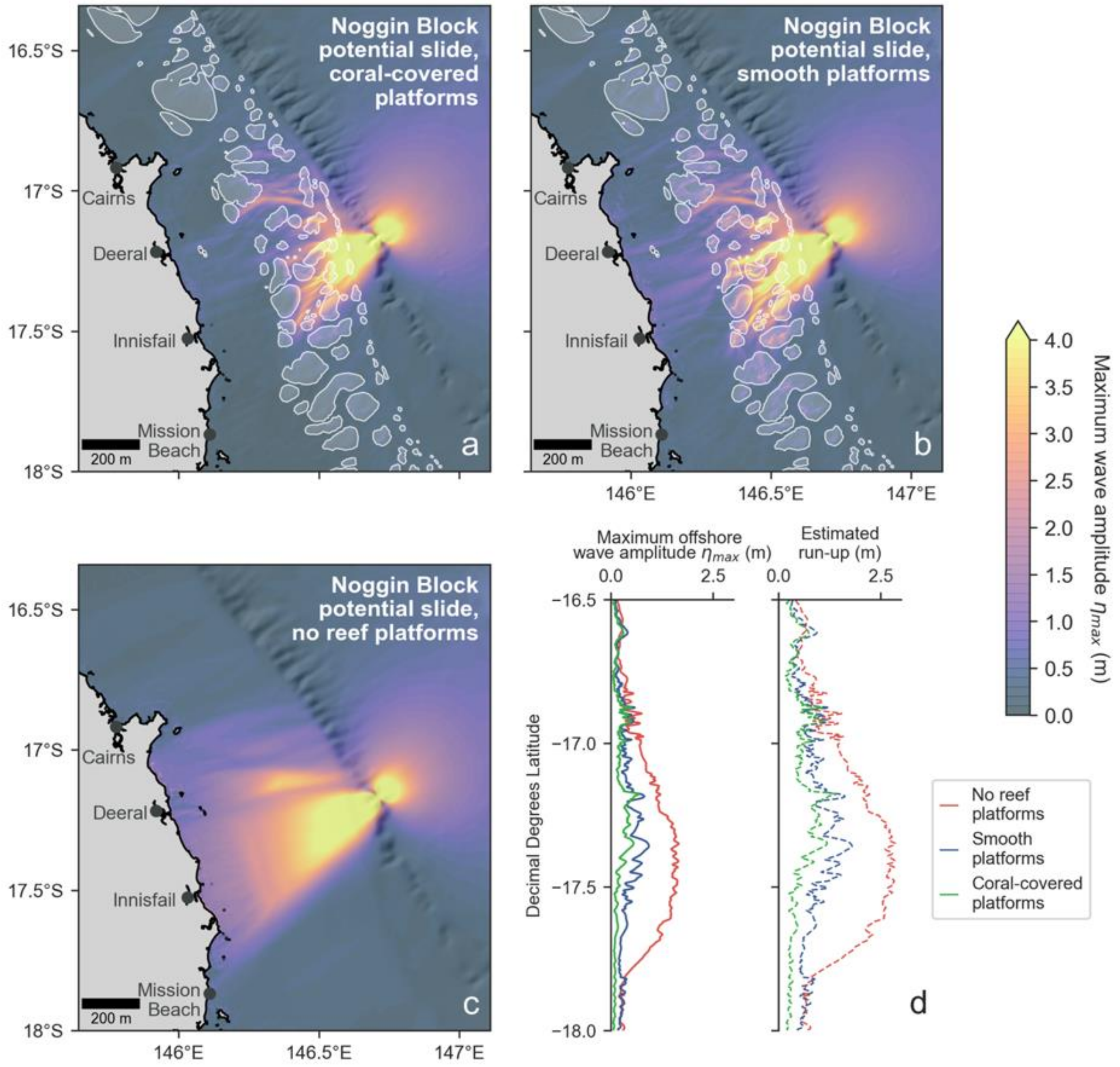

Figure 12. Maximum wave amplitude distributions for the Noggin Block potential landslide scenario simulated with a) the modern "coral-covered platforms" (bottom friction coefficient C_D=0.1522 on platforms, shown in white) b) "smooth platforms" (C_D=0.0025), and c) "no reef platforms". d) Corresponding maximum offshore wave amplitude and estimated run-up distributions. Maximum run-up estimates are ~1.4 m for the "coral-covered platforms" scenario, ~1.8 m for the "smooth platforms" scenario, and ~2.9 m for the "no reef platforms" scenario.

Offshore wave amplitudes were interpolated along the 25 m isobath. For animations of the "coral-covered platforms" and "no reef platforms" scenarios, see Online Resources 7 and 8.

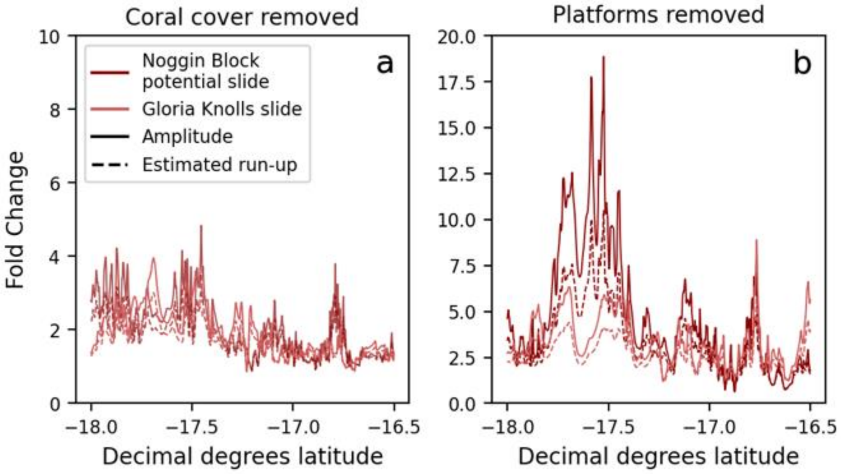

Figure 13. Fold-change increase in both landslide tsunami amplitude and estimated run-up when a) coral cover is removed and b) reef platforms are removed. Amplitudes, which were also used to calculate run-up, were extracted along the 25 m isobath.

4.5. Tidal impacts on tsunami propagation

The additional impact of tide level was tested for the M_w 8.5 Solomon Islands earthquake scenario, the Gloria Knolls Slide scenario, and the Noggin Block potential slide scenario. Results indicate a minimal impact of tide level on the degree of attenuation of the M_w 8.5 earthquake-triggered tsunami (Figure 14a), where amplitudes were 1.6% lower on average at low spring tide (1.75 m below MSL; Figure 14b) and 2.6% higher on average at high spring tide (1.75 m above MSL; Figure 14c). Offshore amplitude and run-up distributions along the 25 m isobath are very similar for all tide cases (Figure 14d). For the Gloria Knolls Slide, the effect of tides is more pronounced, where amplitudes decrease 11 % on average during low spring tide and increase 17% on average at high spring tide (Figure 15). Similarly, for the Noggin Block, potential slide scenario (Figure 16a), amplitudes were 16% lower on average at low spring tide (Figure 16b) and 6% higher on average at high spring tide (Figure 16c).

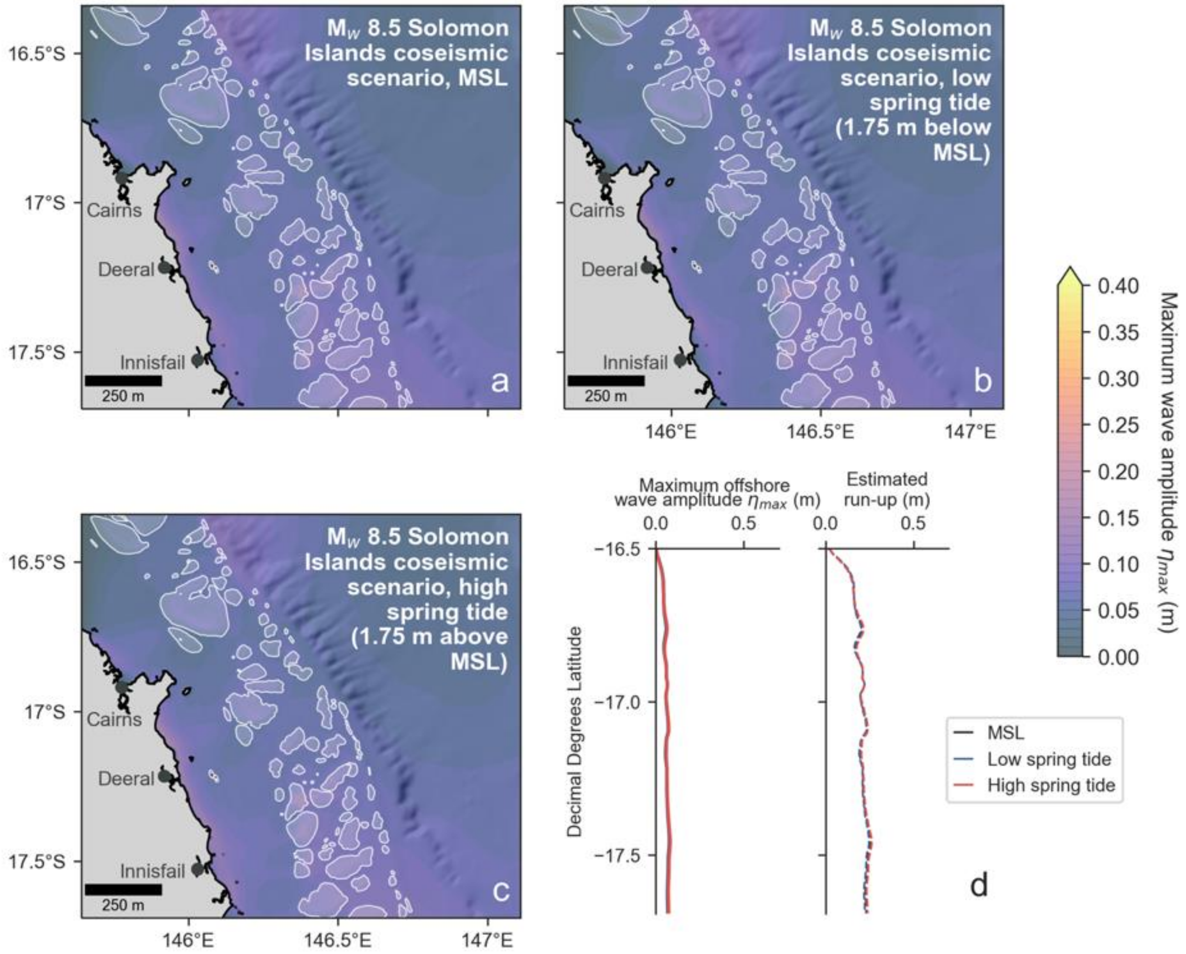

Figure 14. Maximum wave amplitude distributions for the hypothetical M_w 8.5 Solomon Islands earthquake scenario simulated at a) mean sea level (MSL, bottom friction coefficient $C_D=0.1522$ on platforms, shown in white) b) low spring tide (1.75 m below MSL, $C_D=0.1522$ on platforms), and c) high spring tide (1.75 m above MSL, $C_D=0.1522$ on platforms). d) Corresponding maximum offshore wave amplitude and estimated run-up distributions. Maximum run-up estimates are 26 cm for the MSL scenario, 25 cm for the low spring tide scenario, and 26 cm for the high spring tide scenario. Offshore wave amplitudes were interpolated along the 25 m isobath.

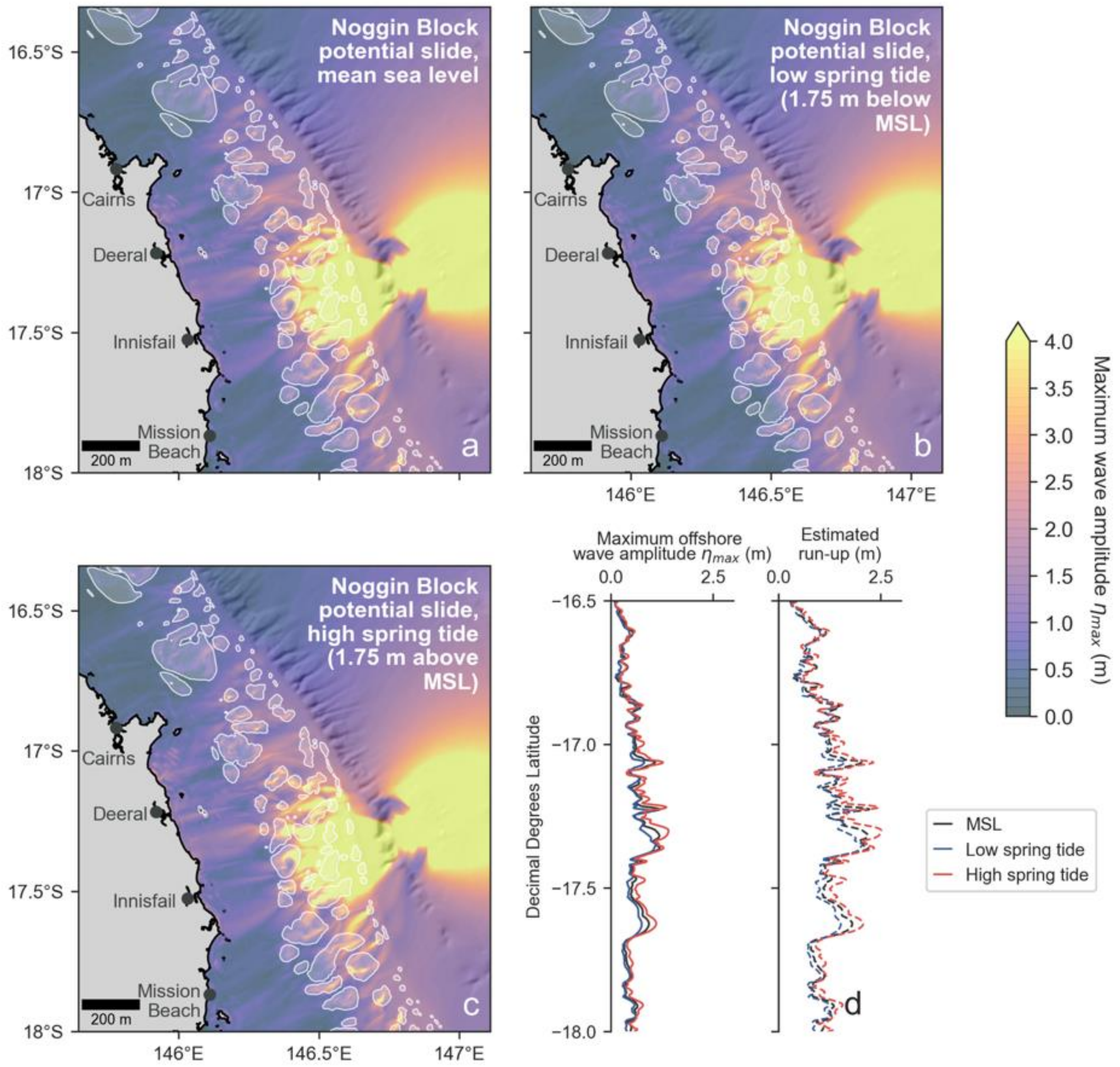

Figure 15. Maximum wave amplitude distributions for the Gloria Knolls Slide scenario simulated at a) mean sea level (bottom friction coefficient C_D=0.1522 on platforms, shown in white) b) low spring tide (1.75 m below MSL, C_D=0.1522 on platforms), and c) high spring tide (1.75 m above MSL, C_D=0.1522 on platforms). d) Corresponding maximum offshore wave amplitude and estimated run-up distributions. Maximum run-up estimates are 1.4 m for the MSL scenario, 1.4 m for the low spring tide scenario, and 1.3 m for the high spring tide scenario. Offshore wave amplitudes were interpolated along the 25 m isobath.

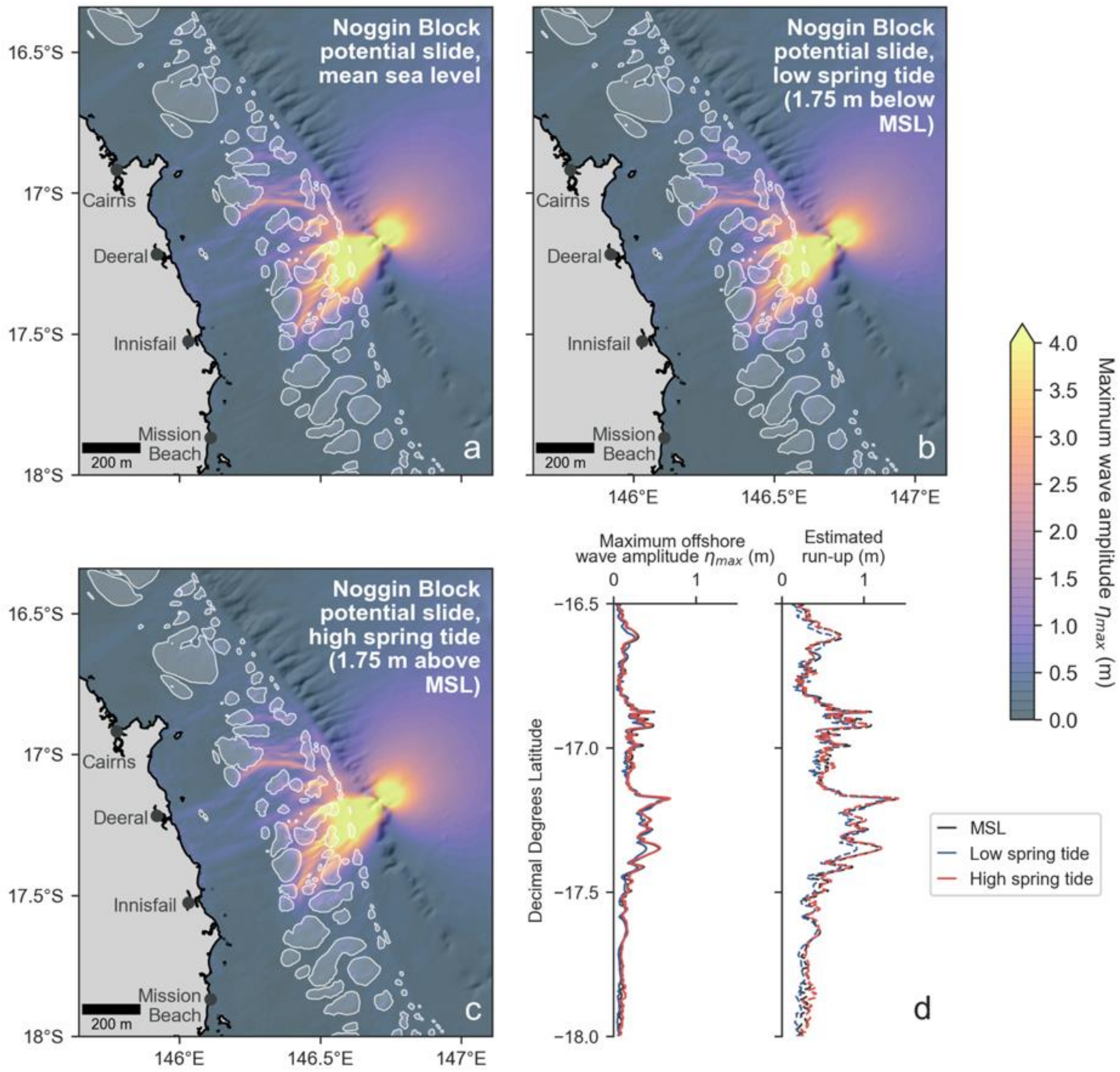

Figure 16. Maximum wave amplitude distributions for the Noggin Block potential slide scenario simulated at a) mean sea level (bottom friction coefficient C_D=0.1522 on platforms, shown in white) b) low spring tide (1.75 m below MSL, C_D=0.1522 on platforms), and c) high spring tide (1.75 m above MSL, C_D=0.1522 on platforms). d) Corresponding maximum offshore wave amplitude and estimated run-up distributions. Maximum run-up estimates are 1.4 m for the MSL scenario, 1.4 m for the low spring tide scenario, and 1.3 m for the high spring tide scenario. Offshore wave amplitudes were interpolated along the 25 m isobath.

5. Discussion

5.1. The impact of the GBR's ecosystem-scale complexity on tsunami propagation

Our results show that tsunamis are strongly impacted by the presence of coral cover in the GBR. Across many of the "coral-covered platforms" simulations, maps showing maximum wave amplitude distributions show clear "shadow zones" landward of reef platforms, where amplitudes markedly decrease. These impacts are especially pronounced for the M_W 9.0 Solomon Islands earthquake scenario (Figure 9), the Gloria Knolls submarine landslide scenario (Figure 11) and the Noggin Block potential submarine landslide scenario (Figure 12). These declines in wave amplitude are driven by elevated frictional dissipation over coral-covered reef platforms. We eliminate the possibility that wave breaking contributed to energy dissipation, as wave-breaking was not detected in any of the simulations due to the tsunamis' large wavelengths in comparison to their amplitudes. These results reaffirm the prevailing notion that the GBR acts as a regional buffer to tsunamis (Baba et al. 2008; Wei et al. 2015; Xing et al. 2015; Webster et al. 2016; Puga-Bernabéu et al. 2019). They are also consistent with previous findings from other modelling studies, especially those that include wider reef platforms in their assessments (Kunkel et al. 2006; Gelfenbaum et al. 2011; Yao et al. 2012), which allows the cumulative impact of frictional dissipation to dominate. Therefore, we propose that the effect of live coral cover should be directly incorporated into future hazard assessments of the northeastern Australian margin, as we anticipate it will have a detrimental impact on propagating tsunamis.

The energy-diminishing impact of coral cover becomes most apparent when comparing the "coral-covered platforms" simulations with the "smooth platforms" simulations. When coral cover is removed, amplitudes increase across each source scenario tested here. Notably, run-up projections increase as much as 24% for the M_w 9.0 earthquake source (Figure 10), and they exhibit a maximum of a nearly four-fold change for the Noggin Block potential slide (Figure 13). These increases in amplitude and run-up imply that while coral cover in the GBR may currently have a buffering effect on tsunami wave energy, this effect may diminish as reef ecosystems in the GBR continue to decline under the physiological stressors (e.g., heat stress, acidity stress) that accompany anthropogenic climate change (Hughes et al. 2018). Generally speaking, the structural complexity of coral reefs is expected to deteriorate as reef-building species are lost and as ecosystems transition to algal-dominated states (Bellwood et al. 2004; Alvarez-Filip et al. 2009; Wild et al. 2011). This deterioration of structural complexity is expected to lessen frictional dissipation of wind wave energy (Harris et al. 2018; de Lalouvière et al. 2020). Based on our results, we expect a similar outlook for tsunami wave hazards. This loss of buffering capacity may be further compounded by the effects of sea level rise, where some assessments have forecasted heightened tsunami hazard under current projections (Li et al. 2018; Nagai et al. 2020).

Across source scenarios, there are prominent discrepancies in the magnitude of the amplitude and run-up increases when coral cover is removed. For instance, while the M_w 8.0 earthquake scenario experiences marginal increases (4% maximum, see Figure 10), M_w 9.0 scenario experiences substantial jumps in offshore amplitude (up to 31%) when platforms are smoothed. This implies that the degree of coral-induced frictional dissipation at bed is different across source scenarios. Our findings demonstrate that these differences in frictional dissipation are directly related to wave amplitude (and thus, wave energy). Particle velocity (note: this is different to wave *celerity*) is a function of wave amplitude (Nielsen 1992), and therefore, waves of differing amplitudes experience different degrees of dissipation due to shear stress at bed. This amplitude-mediated discrepancy in particle velocity is best exemplified by comparing earthquake scenarios, where tsunami amplitude was altered by changing the magnitude and slip displacement of the initial coseismic source (Figure 4, see Table 1 for source parameters). For the M_w 8.0 Solomon Islands earthquake scenario, bed particle velocities are relatively low (< 1 cm/s) throughout the computational domain given the relatively low tsunami amplitudes produced by the source. However, for the M_w 8.5 and M_w 9.0 earthquake scenarios, particle velocities are much higher on the shelf (> 5 cm/s). Moreover, in their corresponding "smooth platforms” simulations, particle velocities are more elevated atop the reef platforms than in the “coral-covered platforms” simulations, which further reflects the dissipative effect of coral cover. As wave energy dissipation through shear stress is proportional to the square of the particle velocity (see Eq. 1), the higher velocities computed for higher-magnitude earthquake tsunamis result in greater overall wave energy dissipation via bottom friction when coral cover is present. This also explains why a relatively large degree of attenuation is observed for the landslide-generated tsunamis, both of which produce similarly high waves (9 m and 3.5 m for the landward-propagating waves, respectively). Our results show that tsunami amplitude, which ultimately depends on the magnitude and proximity of the triggering source, should also be considered when examining the buffering capacity of natural defences such as coral reefs.

While the GBR generally acts as a buffer to tsunami wave energy, despite its namesake, the GBR itself does not form a continuous barrier on the mid- to outer shelf, especially in the central region (Figure 3). As a result, the buffering effect offered by coral cover varies considerably alongshore. Turning again to the Solomon Islands earthquake scenarios (Figure 10), when coral cover is removed, the largest increases in wave amplitude and run-up tend to occur landward of broad reef platforms (see also Figure 9a, b). On the other hand, areas that lie between inter-reef passages, or gaps, exhibit smaller increases in amplitude and run-up. This phenomenon is consistent across source scenarios, and it is particularly pronounced in cases where tsunami amplitudes are relatively high. This implies that the protectiveness offered by coral cover varies alongshore because of platform placement; if coral-covered platforms (particularly broad platforms) are positioned between the incoming tsunami and the shoreline, they are more inclined to dampen the tsunami.

To summarise, reef cover contributes substantially to the overall buffering capacity of the GBR, which is consistent with previous findings (e.g., Kunkel et al. 2006). However, the GBR's buffering capacity for any given location alongshore depends on various site-specific factors, including the presence of coral cover, the relative positioning of the platforms, and tsunami amplitude.

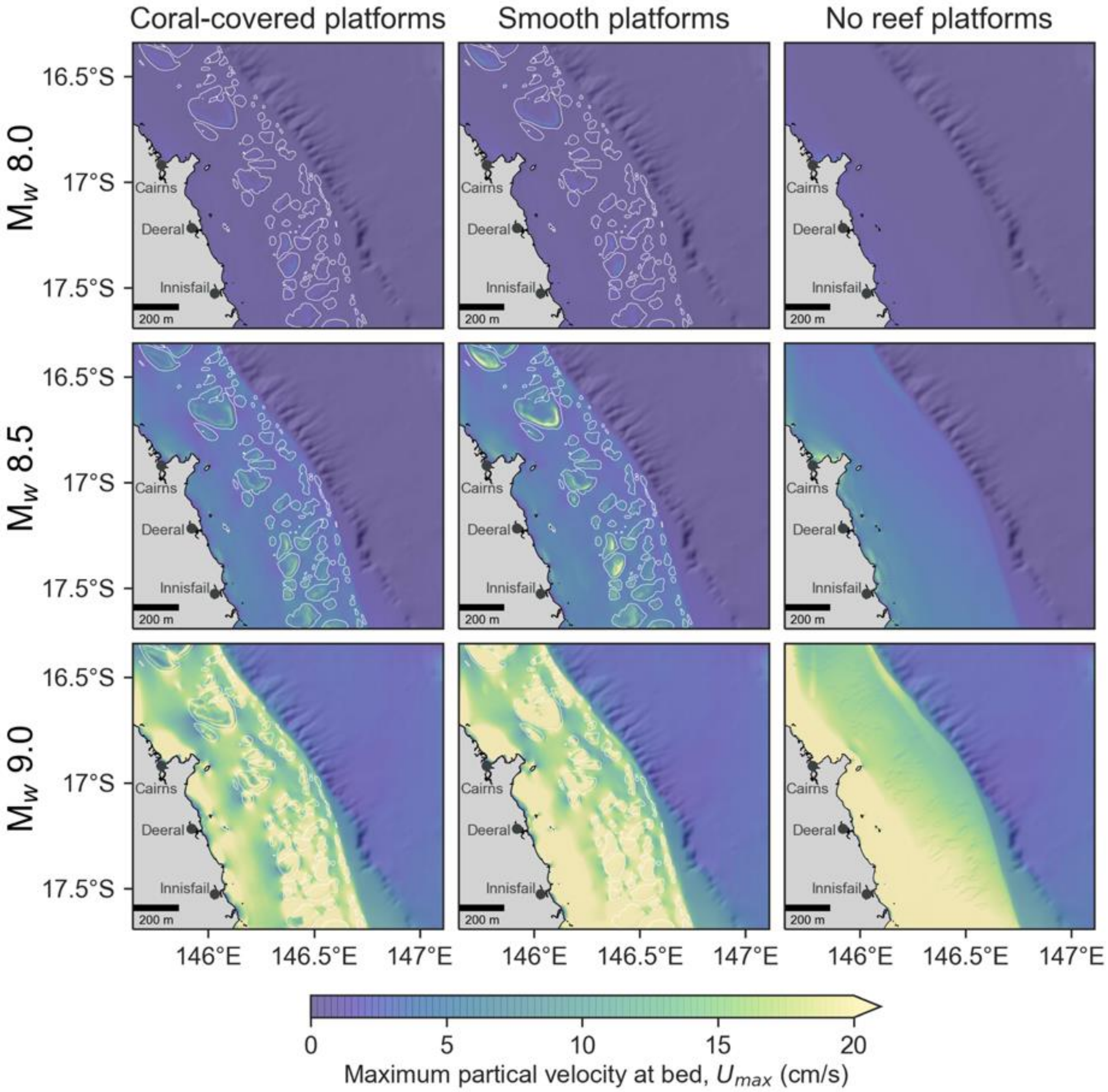

Figure 17. Maximum bed particle velocities (in cm/s) across the computational domain for each the M_w 8.0 Solomon Islands earthquake scenario (top row), the M_w 8.5 scenario (middle row), and the M_w 9.0 scenario (bottom row). Columns are aligned based on their corresponding "coral-covered platforms" simulations (left column), "smooth platforms" simulations (middle column), and "no reef platforms" simulations (right column).

5.2. The impact of the GBR's bathymetric-scale complexity on tsunami propagation

Our simulations reveal the remarkably complex ways in which tsunami waves interact with the larger-scale bathymetric features (i.e., platforms, shoals, etc.) that comprise the GBR. Of particular note is the platforms' ability to focus tsunami wave energy towards shore (see Figure 8 and Online Resource 3 for the M_w 8.5 Solomon Islands earthquake simulations). In a manner analogous to a convex lens focussing light, platforms cause the incoming tsunami waves to refract inwards towards their shallower depths, inciting shoaling, positive wave interference, and subsequent heightening of wave trains. Shoaling and heightening of tsunami waves over shallow reefs has been observed by others, both from field-based and modelling evidence (Chatenoux and Peduzzi 2005; Gelfenbaum et al. 2011). Interestingly, frictional dissipation by coral cover appears to fully or partially counteract these focussing effects, where waves subsequently dampen after growing in amplitude over the platforms (e.g., Figure 9). Consequently, smoothing the domain tends to enhance the platforms' ability to focus wave energy. This is demonstrated by the higher-amplitude, landward wave trains shown in wave amplitude distributions (e.g., Figure 9). Some platforms appear to more effectively focus wave energy than others, and we suspect this is due to factors such as reef morphology, size, and submergence depth. A more systematic investigation of platform characteristics warranted to test this hypothesis, particularly as coral reef cover is expected to decline in the future.

In addition to focussing effects, simulated tsunamis exhibit a complex interplay of additional behaviours when interacting with platforms, such as diffraction, reflection, and scattering of wave trains (see Online Resource 5 for example). These effects are most pronounced for the landslide-generated tsunami cases (see Section 4.4), and we tentatively suggest that this is due to their shorter wavelengths. Our simulations further reinforce the important role that local bathymetry plays in modulating tsunami behaviour, particularly in shallow reef environments

(Baba et al. 2008; Dilmen et al. 2018). This potent, complex, and site-specific control on tsunami propagation further underscores the need to evaluate tsunami hazard on a case-by-case basis.

We also highlight the intriguing role of inter-reef passages, or gaps, in modulating tsunami behaviour as it crosses the shelf. Many have hypothesized that gaps in the reef structure worsen the tsunami hazard, as the gaps act as low-resistance conduits that amplify wave energy (Nott 1997; Liu et al. 2005; Gelfenbaum et al. 2011; McAdoo et al. 2011; Roger et al. 2014). In our simulations, porous gaps in the reef structure certainly permit wave energy to pass through to the coastline. However, there is little evidence to support the notion that the gaps amplify waves. In fact, due to focussing, amplification of wave amplitudes occurs *over* the platforms rather than *between* them (e.g., Figure 9, Figure 11). In the case of the GBR, many of the platforms appear to be wide enough, deep enough, far enough apart, and far enough from the coastline such that the inter-reef gaps do not pose a significant hazard. This is in contrast to many fringing reef systems, where gaps can be quite narrow, shallow, and close to shore. We therefore suggest that for the GBR, the wave focussing ability of platforms may be of greater concern for the northeastern Australian coastline than the presence of gaps in the reef structure.

Overall, the GBR's underlying bathymetric structure contributes significantly to its buffering capacity, and this becomes apparent when platforms are removed from simulations (see Figure 10 and Figure 13). When platforms are removed, waves are permitted to propagate smoothly and uninterruptedly across the shelf, highlighting the highly obstructive nature of the platforms themselves. Offshore wave amplitudes and run-up distributions increase alongshore across all source scenarios when platforms are removed. These findings are consistent with previous work which suggests that bathymetric irregularities on the shelf exert large control on the eventual run-up distribution at the coast (Baba et al. 2008; Schambach et al. 2018). Even as the GBR is interrupted by gaps, the presence reef structure appears to provide at least some benefit to nearly all areas of the coastline examined in this study.

5.3. Broader implications surrounding the GBR’s impact on tsunami hazard

This study has revealed wider implications for communities situated along the northeastern Australian coastline. Firstly, from a mitigation perspective, the GBR may offer greater protection for more severe tsunami events. In particular, the GBR may offer natural protection against near-field landslide sources, which are notoriously difficult to predict and forecast (Tappin et al. 1999; Harbitz et al. 2014). While this may take some pressure off warning systems, we stress that coastal communities should not rely upon the GBR alone to reduce their vulnerability to tsunami hazards. A holistic strategy for tsunami hazard preparedness ultimately should include risk awareness, hazard education, resilient infrastructure, and robust early warning systems (Baird et al. 2005; Liu et al. 2005; Dominey-Howes et al. 2007; Mori et al. 2011).

Secondly, from a *future* mitigation perspective, our work suggests that the declining coral health, which is associated with globally-mediated anthropogenic climate change (De’ath et al. 2012; Hughes et al. 2018), will have an overall adverse effect on the GBR’s defensive capability. In this context, today’s reef-buffering asset may be tomorrow’s liability. Areas of shoreline that are best-protected by broad, expansive coral-covered platforms may experience the highest inundation risk in the future as coral die-off continues and as architectural complexity deteriorates (Alvarez-Filip et al. 2009), enhancing the platforms’ ability to focus energy towards shore rather than attenuating it. These local differences reinforce the need for site-specific hazard assessments when considering tsunami hazard on the northeastern Australian margin in the future.

5.4. Reconciling differing interpretations of coral reef impact on tsunamis

In light of our results, we address some of the contrasting interpretations in the literature around the impact of coral reefs on tsunami hazard. Firstly, while the GBR, being an offshore barrier system, buffers the tsunami hazard for the more distant Australian coastline, other reef environments (in particular, narrow fringing reefs that surround populated inner islands) could exacerbate tsunami hazard through behaviours such as shoaling, focussing, and bore formation (Chatenoux and Peduzzi 2005; Fritz et al. 2011; Gelfenbaum et al. 2011; Yao et al. 2012). Indeed, our simulations showcase shoaling and focussing on platforms, which locally augment wave amplitudes at the intra-platform scale. A more rigorous inundation study would be needed to confirm whether this translates to increased hazard within the lagoons, shoals, and islands that rest within the platforms. Therefore, coral reefs could have either beneficial or detrimental effects on the overall hazard depending on the type reef system in question and the proximity of coastal communities and assets to the site of the most severe shoaling/focussing. In the debate surrounding reef protectiveness against tsunamis, a distinction must be made between fringing reef systems and offshore barrier systems, as they have different implications for proximity to wave focussing effects, and therefore, exposure.

On the other hand, we also note potential ambiguities around the ways in which the impact of coral reefs is reported in post-tsunami field surveys. From our simulations and others (Kunkel et al. 2006; Uslu et al. 2010; Gelfenbaum et al. 2011), there is evidently a strong theoretical basis to support the fact that coral reefs can dissipate tsunami wave energy, reducing the tsunami *hazard*. However, this overall reduction in hazard may not be sufficient to completely reduce the *physical vulnerability* and *exposure* of coastal communities (Uslu et al. 2010). When discussing the buffering role of reefs, many have highlighted that despite being within close proximity to reefs, coastal assets have nonetheless been destroyed during tsunami events (e.g., Baird et al. 2005), leading some to conclude that coral reefs provide no protective benefit to coastal communities. In these cases, the reefs could very well have buffered the overall tsunami hazard, reducing the overall inundation and run-up extent. However, this protective benefit may not have been sufficient to completely shield coastal communities that were situated close to shore. Care must be taken when retrospectively interpreting the role that coral reefs may have played in reducing tsunami hazard along a shoreline, and a clear distinction should be made between *hazard reduction* and *risk reduction*, which lies at the intersection between hazard, exposure, and vulnerability.

5.5. Study limitations and future work

Uncertainties persist that could complicate such future tsunami hazards assessments in coral reef environments. Firstly, at the ecosystem-scale, the relationship between coral rugosity and community composition requires more precise quantification on an intra-reef platform scale (Rogers et al. 2016). This will continue to be a pressing task in the future, as profound ecological shifts may be precipitated by both the immediate aftermath of the tsunami impact and longer-term environmental changes, thus affecting ecosystem-scale structural complexity (Madin and Connolly 2006; Alvarez-Filip et al. 2009; Ferrari et al. 2016; Hughes et al. 2018). While platform degradation and bioerosion is largely anticipated to flatten coral reefs (Alvarez-Filip et al. 2009), the shorter-term impact of these and other stressors on ecosystem-scale rugosity is still not precisely known. These ecosystems should be stringently monitored to better assess how coastal hazard severity as a whole will be transformed in these areas. Additionally, the approach used to parameterize bottom shear stress, though very common both in the field and in modelling studies, may need to be reconfigured to account for more complex tsunami interactions and subgrid turbulent dissipation within the 3D reef structure (Lowe et al. 2008; Kim et al. 2009; Rosman and Hench 2011). Moreover, these more complex interactions may be better represented by a Navier Stokes model rather than a depth-averaged wave model (Kazolea et al. 2019).

On a larger scale, it is worth exploring the potential impact of undular bores that could arise and break on the platforms themselves, as they could play an additional role in dissipating wave energy offshore (Grilli et al. 2012; Glimsdal et al. 2013). These wave features would not have been resolved in our coarser-resolution runs (Schambach et al. 2018), as capturing them quickly becomes very demanding computationally (<10 m resolution required, Grilli et al. 2012). Also, while our study emphasizes the effect of the GBR on offshore amplitudes and projected run-up distributions, ultimately, tsunami-induced surges and bores deliver the force and high water levels that cause destruction to coastal communities onshore (Koshimura et al. 2009; Nistor et al. 2009; Nouri et al. 2010). Further work is warranted to establish whether the reduction in offshore wave amplitude translates to a reduced hazard onshore, and this would necessitate the deployment of higher-resolution inundation simulations.

Finally, our study was not designed to provide a reappraised, comprehensive hazard assessment for the northeastern Australian coastline although our findings suggest that the reef's role should be considered in future assessments. That being said, we stress the need for a robust parameterization of reef roughness (Nelson 1996; Rosman and Hench 2011). Furthermore, as indicated by sensitivity analyses (see Online Resource 2), these propagation simulations require high spatial resolution (200 m for earthquake sources and 100 m or less for landslide sources) in order to properly capture the reef structure and to resolve complex tsunami-reef interactions. While this increases computational demand, we nonetheless deem it worthwhile to consider the role of the reef, as current assessments may be over-estimating tsunami risk in northeast Australia. Additionally, a more meaningful assessment of the submarine landslide tsunami hazard is needed to better understand the timing, frequency, and magnitude of these events. In the future, it may be worth considering more complex failure dynamics (i.e. landslide deformation and two-way coupling with the water column), which could alter the run-up results (Masson et al. 2006; Geist et al. 2009; Abadie et al. 2010), but we anticipate that accounting for these dynamics will not alter the overall conclusions established here about the buffering effect of the GBR. Addressing these limitations will enable more reliable forecasting as the fate of the world's coral reefs becomes clearer with time.

6. Conclusions

This study demonstrates the nuanced interactions between tsunamis and coral reef systems. In agreement with previous work we find that the Great Barrier Reef (GBR), both in terms of coral cover and larger-scale bathymetric complexity, acts as a large-scale regional buffer against tsunamis. However, the reef appears to provide greater protection against higher-amplitude tsunamis due to the larger computed particle velocities at bed, which directly dictates the degree of frictional dissipation through shear stress. Additionally, we find that the protectiveness offered by the GBR locally depends on coral cover and platform distribution. We also find that wave focussing by reef platforms could pose a greater hazard than the gaps between platforms, which have been previously thought to amplify waves. In the context of the larger debate about whether coral reefs reduce tsunami hazards for coastal communities, we conclude that differing interpretations can be reconciled when considering site-specific factors.

Acknowledgements

We extend our sincere gratitude to Fengyan Shi for his assistance with model set-up and troubleshooting. We also thank Lorena Moscardelli for allowing us to reproduce a significant portion of her submarine landslide database for this work. We are grateful to Tristan Salles, Jon Hill, and Greg Houseman for their constructive and insightful comments. Stewart Allen and Diana Greensdale from the Australian Bureau of Meteorology provided earthquake source parameters. Computational resources were provided by the National Computational Infrastructure (NCI) in Canberra, Australia, which is supported by the Australian Commonwealth Government. We also thank the Sydney Informatics Hub at the University of Sydney for the provisioning of both expertise and computing power by their high-performance computing facility (Artemis).

References

Abadie S, Morichon D, Grilli S, Glockner S (2010) Numerical simulation of waves generated by landslides using a multiple-fluid Navier–Stokes model. Coast Eng 57:779–794. https://doi.org/10.1016/j.coastaleng.2010.03.003

Aksu AE, Hiscott RN (1992) Shingled Quaternary debris flow lenses on the north-east Newfoundland Slope. Sedimentology 39:193–206. https://doi.org/10.1111/j.1365-3091.1992.tb01034.x

Alfaro E, Holz M (2014) Seismic geomorphological analysis of deepwater gravity-driven deposits on a slope system of the southern Colombian Caribbean margin. Mar Pet Geol 57:294–311. https://doi.org/10.1016/j.marpetgeo.2014.06.002

Alvarez-Filip L, Dulvy NK, Gill JA, et al (2009) Flattening of Caribbean coral reefs: region-wide declines in architectural complexity. Proc R Soc B Biol Sci 276:3019–3025. https://doi.org/10.1098/rspb.2009.0339

Alves TM, Cartwright JA (2009) Volume balance of a submarine landslide in the Espírito Santo Basin, offshore Brazil: quantifying seafloor erosion, sediment accumulation and depletion. Earth Planet Sci Lett 288:572–580. https://doi.org/10.1016/j.epsl.2009.10.020

Amante C, Eakins BW (2009) ETOPO1 Arc-Minute Global Relief Model: Procedures, Data Sources and Analysis. NOAA Technical Memorandum NESDIS NGDC-24. National Geophysical Data Center, NOAA

Andrews JC, Bode L (1988) The tides of the central Great Barrier Reef. Cont Shelf Res 8:1057–1085. https://doi.org/10.1016/0278-4343(88)90039-8

Ashabranner LB, Tripsanas EK, Shipp RC (2010) Multi-direction Flow in a Mass-Transport Deposit, Santos Basin, Offshore Brazil. In: Mosher DC, Shipp RC, Moscardelli L, et al. (eds) Submarine Mass Movements and Their Consequences. Springer Netherlands, Dordrecht, pp 247–255

Australian Bureau of Meteorology (2020) Past Tsunami Events. http://www.bom.gov.au/tsunami/history/index.shtml

Baba T, Mleczko R, Burbidge D, et al (2008) The effect of the great barrier reef on the propagation of the 2007 Solomon Islands tsunami recorded in Northeastern Australia. Pure Appl Geophys 165:2003–2018. https://doi.org/10.1007/s00024-008-0418-5

Baird AH, Campbell SJ, Anggoro AW, et al (2005) Acehnese Reefs in the Wake of the Asian Tsunami Centre for Coral Reef Biodiversity. Curr Biol 15:1926–1930. https://doi.org/10.1016/j.cub.2005.09.036

Barnes PM, Lewis KB (1991) Sheet slides and rotational failures on a convergent margin: the Kidnappers Slide, New Zealand. Sedimentology 38:205–221. https://doi.org/10.1111/j.1365-3091.1991.tb01257.x

Beaman RJ (2010) Project 3D-GBR: A high-resolution depth model for the Great Barrier Reef and Coral Sea. Project 2.5i.1a Final Report, Marine and Tropical Sciences Research Facility, Cairns, Australia

Behrmann JH, Völker D, Geersen J, et al (2014) Size-Frequency Relationship of Submarine Landslides at Convergent Plate Margins: Implications for Hazard and Risk Assessment. In: Krastel S, Behrmann J-H, Völker D, et al. (eds) Submarine Mass Movements and Their Consequences: 6th International Symposium. Springer International Publishing, Cham, pp 165–175

Bellwood DR, Hughes TP, Folke C, Nyström M (2004) Confronting the coral reef crisis. Nature 429:827–833. https://doi.org/10.1038/nature02691

Boudon G, Le Friant A, Komorowski J, et al (2007) Volcano flank instability in the Lesser Antilles Arc: diversity of scale, processes, and temporal recurrence. J Geophys Res Solid Earth 112:B08205. https://doi.org/10.1029/2006JB004674

Bourget J, Zaragosi S, Rodriguez M, et al (2013) Late Quaternary megaturbidites of the Indus Fan: Origin and stratigraphic significance. Mar Geol 336:10–23. https://doi.org/10.1016/j.margeo.2012.11.011

Bourget J, Zaragosi S, Ellouz-Zimmermann N, et al (2011) Turbidite system architecture and sedimentary processes along topographically complex slopes: the Makran convergent margin. Sedimentology 58:376–406. https://doi.org/10.1111/j.1365-3091.2010.01168.x

Boyd R, Keene J, Hubble T, et al (2010) Southeast Australia: A Cenozoic Continental Margin Dominated by Mass Transport. In: Submarine Mass Movements and Their Consequences. pp 491–502

Bozec Y-M, Alvarez-Filip L, Mumby PJ (2015) The dynamics of architectural complexity on coral reefs under climate change. Glob Chang Biol 21:223–235. https://doi.org/10.1111/gcb.12698

Brune S, Babeyko a. Y, Ladage S, Sobolev S V. (2010) Landslide tsunami hazard in the Indonesian Sunda Arc. Nat Hazards Earth Syst Sci 10:589–604. https://doi.org/10.5194/nhess-10-589-2010

Burke L, Reytar K, Spalding M, Perry A (2011) Reefs at risk revisited. World Resources Institute, Washington, DC

Calvès G, Huuse M, Clift PD, Brusset S (2015) Giant fossil mass wasting off the coast of West India: The Nataraja submarine slide. Earth Planet Sci Lett 432:265–272. https://doi.org/10.1016/j.epsl.2015.10.022

Camerlenghi A, Accettella D, Costa S, et al (2009) Morphogenesis of the SW Balearic continental slope and adjacent abyssal plain, Western Mediterranean Sea. Int J Earth Sci 98:735. https://doi.org/10.1007/s00531-008-0354-8

Campbell DC, Mosher DC (2010) Middle to Late Miocene Slope Failure and the Generation of a Regional Unconformity Beneath the Western Scotian Slope, Eastern Canada BT - Submarine Mass Movements and Their Consequences. In: Mosher DC, Shipp RC, Moscardelli L, et al. (eds). Springer Netherlands, Dordrecht, pp 645–655

Canals M, Lastras G, Urgeles R, et al (2004) Slope failure dynamics and impacts from seafloor and shallow sub-seafloor geophysical data: case studies from the COSTA project. Mar Geol 213:9–72. https://doi.org/10.1016/j.margeo.2004.10.001

Carlson PR, Karl HA, Edwards BD, et al (1993) Mass movement related to large submarine canyons along the Beringian Margin, Alaska. In: Submarine Landslides: Selected Studies in the US Exclusive Economic Zone. U.S. Geological Survey Bulletin, Washington, DC, p 104

Center for International Earth Science Information Network (CIESIN) (2018) Gridded Population of the World, Version 4 (GPWv4): Population Density Adjusted to Match 2015 Revision UN WPP Country Totals, Revision 11. NASA Socioeconomic Data and Applications Center (SEDAC), Columbia University, Palisades, NY

Chatenoux B, Peduzzi P (2005) Analysis on the Role of Bathymetry and other Environmental Parameters in the Impacts from the 2004 Indian Ocean Tsunami. UNEP/GRID-Europe, Geneva

Chatenoux B, Peduzzi P (2007) Impacts from the 2004 Indian Ocean Tsunami: Analysing the potential protecting role of environmental features. Nat Hazards 40:289–304. https://doi.org/10.1007/s11069-006-0015-9

Chaytor JD, Twichell DC, Lynett P, Geist EL (2010) Distribution and Tsunamigenic Potential of Submarine Landslides in the Gulf of Mexico. In: Mosher DC, Shipp RC, Moscardelli L, et al. (eds) Submarine Mass Movements and Their Consequences. Springer Netherlands, Dordrecht, pp 745–754

Chaytor JD, Geist EL, Paull CK, et al (2016) Source Characterization and Tsunami Modeling of Submarine Landslides Along the Yucatán Shelf/Campeche Escarpment, Southern Gulf of Mexico. Pure Appl Geophys 173:4101–4116. https://doi.org/10.1007/s00024-016-1363-3

Chaytor JD, ten Brink US, Solow AR, Andrews BD (2009) Size distribution of submarine landslides along the U.S. Atlantic margin. Mar Geol 264:16–27. https://doi.org/10.1016/j.margeo.2008.08.007

Chaytor JD, Twichell DC, ten Brink US (2012) A Reevaluation of the Munson-Nygren-Retriever Submarine Landslide Complex, Georges Bank Lower Slope, Western North Atlantic. In: Yamada Y, Kawamura K, Ikehara K, et al. (eds) Submarine Mass Movements and Their Consequences. Springer Netherlands, Dordrecht, pp 135–146

Collot J, Lewis K, Lamarche G, Lallemand S (2001) The giant Ruatoria debris avalanche on the northern Hikurangi margin, New Zealand: Result of oblique seamount subduction. J Geophys Res Solid Earth 106:19271–19297. https://doi.org/10.1029/2001JB900004

Dalla Valle G, Gamberi F, Foglini F, Trincardi F (2015) The Gondola Slide: A mass transport complex controlled by margin topography (South-Western Adriatic Margin, Mediterranean Sea). Mar Geol 366:97–113. https://doi.org/10.1016/j.margeo.2015.05.001

Davies G, Griffin J (2018) The 2018 Australian Probabilistic Tsunami Hazard Assessment: Hazard from Earthquake Generated Tsunamis. Geoscience Australia, Canberra

Davies PJ, McKenzie JA, Palmer-Julson AA, et al (1991) Site 819. In: McKenzie JA, Palmer-Julson AA, Betzler C, et al. (eds) Proceedings of the Ocean Drilling Program, Part A: Initial Reports. College Station: TX (Ocean Drilling Program), p 451

De'ath G, Fabricius KE, Sweatman H, Puotinen M (2012) The 27-year decline of coral cover on the Great Barrier Reef and its causes. Proc Natl Acad Sci U S A 109:17995–17999. https://doi.org/10.1073/pnas.1208909109

Dillon WP, Risch JS, Scanlon KM, et al (1993) Ancient crustal fractures control the location and size of collapsed blocks at the Blake Escarpment, east of Florida. In: Schwab W, Lee H, Twichell D (eds) Submarine landslides: Selected Studies in the US Exclusive Economic Zone. US Geological Survey Bulletin, pp 54–59

de Lalouvière C la H, Gracia V, Sierra JP, et al (2020) Impact of Climate Change on Nearshore Waves at a Beach Protected by a Barrier Reef. Water 12:1681

Dilmen DI, Roe GH, Wei Y, Titov V V (2018) The Role of Near-Shore Bathymetry During Tsunami Inundation in a Reef Island Setting: A Case Study of Tutuila Island. Pure Appl Geophys 175:1239–1256. https://doi.org/10.1007/s00024-018-1769-1

Dingle R V (1980) Large allochthonous sediment masses and their role in the construction of the continental slope and rise off southwestern Africa. Mar Geol 37:333–354. https://doi.org/10.1016/0025-3227(80)90109-7

Dingle R V (1977) The anatomy of a large submarine slump on a sheared continental margin (SE Africa). J Geol Soc London 134:293–310. https://doi.org/10.1144/gsjgs.134.3.0293

Dominey-Howes D (2007) Geological and historical records of tsunami in Australia. Mar Geol 239:99–123. https://doi.org/10.1016/j.margeo.2007.01.010

Dominey-Howes D, Papathoma-Köhle M, Bird D, et al (2007) Letter to the Editor: the Australian Tsunami Warning System and lessons from the 2 April 2007 Solomon Islands tsunami alert in Australia. Nat Hazards Earth Syst Sci 7:571–572

Droz L, Dos Reis AT, Rabineau M, et al (2006) Quaternary turbidite systems on the northern margins of the Balearic Basin (Western Mediterranean): a synthesis. Geo-Marine Lett 26:347–359

Eichhubl P, Greene HG, Maher N (2002) Physiography of an active transpressive margin basin: high-resolution bathymetry of the Santa Barbara basin, Southern California continental borderland. Mar Geol 184:95–120. https://doi.org/10.1016/S0025-3227(01)00280-8

Elger J, Berndt C, Krastel S, et al (2015) The Fram Slide off Svalbard: a submarine landslide on a low-sedimentation-rate glacial continental margin. J Geol Soc London 172:153–156. https://doi.org/10.1144/jgs2014-055

Elmore RD, Pilkey OH, Clearly WJ, Curran HA (1979) Black Shell turbidite, Hatteras Abyssal Plain, western Atlantic Ocean. Geol Soc Am Bull 90:1165–1176. https://doi.org/10.1130/0016-7606(1979)90<1165:BSTHAP>2.0.CO;2

Elverhøi A, de Blasio F V, Butt FA, et al (2002) Submarine mass-wasting on glacially-influenced continental slopes: processes and dynamics. Geol Soc London, Spec Publ 203:73–87. https://doi.org/10.1144/GSL.SP.2002.203.01.05

Embley RW (1982) Anatomy of some Atlantic margin sediment slides and some comments on ages and mechanisms. In: Marine Slides and Other Mass Movements. Springer, pp 189–213

Enet F, Grilli ST (2007) Experimental study of tsunami generation by three-dimensional rigid underwater landslides. J Waterw Port, Coastal, Ocean Eng 133:442–454. https://doi.org/10.1061/(ASCE)0733-950X(2007)133:6(442)

Fernando HJS, McCulley JL, Mendis SG, Perera K (2005) Coral poaching worsens tsunami destruction in Sri Lanka. Eos, Trans Am Geophys Union 86:301–304. https://doi.org/10.1029/2005EO330002

Ferrari R, Bryson M, Bridge T, et al (2016) Quantifying the response of structural complexity and community composition to environmental change in marine communities. Glob

Chang Biol 22:1965–1975. https://doi.org/10.1111/gcb.13197

Ferrario F, Beck MW, Storlazzi CD, et al (2014) The effectiveness of coral reefs for coastal hazard risk reduction and adaptation. Nat Commun 5:3794. https://doi.org/10.1038/ncomms4794

Fine I V, Rabinovich AB, Bornhold BD, et al (2005) The Grand Banks landslide-generated tsunami of November 18, 1929: preliminary analysis and numerical modeling. Mar Geol 215:45–57. https://doi.org/10.1016/j.margeo.2004.11.007

Ford M, Becker JM, Merrifield MA, Song YT (2014) Marshall Islands Fringing Reef and Atoll Lagoon Observations of the Tohoku Tsunami. Pure Appl Geophys 171:3351–3363. https://doi.org/10.1007/s00024-013-0757-8

Freire F, Gyllencreutz R, Jafri RU, Jakobsson M (2014) Acoustic evidence of a submarine slide in the deepest part of the Arctic, the Molloy Hole. Geo-Marine Lett 34:315–325

Frey-Martínez J, Cartwright J, James D (2006) Frontally confined versus frontally emergent submarine landslides: a 3D seismic characterisation. Mar Pet Geol 23:585–604. https://doi.org/10.1016/j.marpetgeo.2006.04.002

Fritz HM, Borrero JC, Synolakis CE, et al (2011) Insights on the 2009 South Pacific tsunami in Samoa and Tonga from field surveys and numerical simulations. Earth-Science Rev 107:66–75. https://doi.org/10.1016/j.earscirev.2011.03.004

Fryer GJ, Watts P, Pratson LF (2004) Source of the great tsunami of 1 April 1946: a landslide in the upper Aleutian forearc. Mar Geol 203:201–218. https://doi.org/10.1016/S0025-3227(03)00305-0

Fujii Y, Satake K, Sakai S, et al (2011) Tsunami source of the 2011 off the Pacific coast of Tohoku Earthquake. Earth, Planets Sp 63:55. https://doi.org/10.5047/eps.2011.06.010

Gallop SL, Young IR, Ranasinghe R, et al (2014) The large-scale influence of the Great Barrier Reef matrix on wave attenuation. Coral Reefs 33:1167–1178. https://doi.org/10.1007/s00338-014-1205-7

Gamberi F, Rovere M, Marani M (2011) Mass-transport complex evolution in a tectonically active margin (Gioia Basin, Southeastern Tyrrhenian Sea). Mar Geol 279:98–110. https://doi.org/10.1016/j.margeo.2010.10.015

Gardner J V, Prior DB, Field ME (1999) Humboldt slide—a large shear-dominated retrogressive slope failure. Mar Geol 154:323–338. https://doi.org/10.1016/S0025-3227(98)00121-2

Garziglia S, Sultan N, Cattaneo A, et al (2010) Identification of Shear Zones and Their Causal Mechanisms Using a Combination of Cone Penetration Tests and Seismic Data in the Eastern Niger Delta. In: Mosher DC, Shipp RC, Moscardelli L, et al. (eds) Submarine Mass Movements and Their Consequences. Springer Netherlands, Dordrecht, pp 55–65

Garziglia S, Sultan N, Cattaneo A, et al (2010) Identification of Shear Zones and Their Causal Mechanisms Using a Combination of Cone Penetration Tests and Seismic Data in the Eastern Niger Delta. In: Mosher DC, Shipp RC, Moscardelli L, et al. (eds) Submarine Mass Movements and Their Consequences. Springer Netherlands, Dordrecht, pp 55–65

Gaullier V, Loncke L, Droz L, et al (2010) Slope instability on the French Guiana transform margin from swath-bathymetry and 3.5 kHz echograms. In: Submarine Mass Movements and Their Consequences. Springer, pp 569–579

Gee MJR, Gawthorpe RL, Friedmann SJ (2006) Triggering and evolution of a giant submarine landslide, offshore Angola, revealed by 3D seismic stratigraphy and geomorphology. J Sediment Res 76:9–19. https://doi.org/10.2110/jsr.2006.02

Gee MJR, Uy HS, Warren J, et al (2007) The Brunei slide: a giant submarine landslide on the North West Borneo Margin revealed by 3D seismic data. Mar Geol 246:9–23. https://doi.org/10.1016/j.margeo.2007.07.009

Geersen J, Völker D, Behrmann JH, et al (2011) Pleistocene giant slope failures offshore Arauco peninsula, southern Chile. J Geol Soc London 168:1237–1248. https://doi.org/10.1144/0016-76492011-027

Geist EL, Lynett PJ, Chaytor JD (2009) Hydrodynamic modeling of tsunamis from the Currituck landslide. Mar Geol 264:41–52. https://doi.org/10.1016/j.margeo.2008.09.005

Gelfenbaum G, Apotsos A, Stevens AW, Jaffe B (2011) Effects of fringing reefs on tsunami inundation: American Samoa. Earth-Science Rev 107:12–22. https://doi.org/10.1016/j.earscirev.2010.12.005

Georgiopoulou A, Masson DG, Wynn RB, Krastel S (2010) Sahara Slide: Age, initiation, and processes of a giant submarine slide. Geochemistry, Geophys Geosystems 11:. https://doi.org/10.1029/2010GC003066

Giles MK, Mosher DC, Piper DJW, Wach GD (2010) Mass transport deposits on the southwestern Newfoundland Slope. In: Submarine Mass Movements and Their Consequences. Springer, pp 657–665

Glimsdal S, Pedersen GK, Harbitz CB, Løvholt F (2013) Dispersion of tsunamis: does it really matter? Nat Hazards Earth Syst Sci 13:1507–1526. https://doi.org/10.5194/nhess-13-1507-2013

Goldfinger C, Kulm LD, McNeill LC, Watts P (2000) Super-scale failure of the southern Oregon Cascadia margin. Pure Appl Geophys 157:1189–1226. https://doi.org/10.1007/s000240050023

Graham NAJ, Nash KL (2013) The importance of structural complexity in coral reef ecosystems. Coral Reefs 32:315–326. https://doi.org/10.1007/s00338-012-0984-y

Grantz A, Phillips RL, Mullen MW, et al (1996) Character, paleoenvironment, rate of accumulation, and evidence for seismic triggering of Holocene turbidites, Canada Abyssal Plain, Arctic Ocean. Mar Geol 133:51–73. https://doi.org/10.1016/0025-3227(96)00015-1

Greenslade DJM, Simanjuntak MA, Allen SCR (2009) An enhanced tsunami scenario database: T2. Center for Australian Weather and Climate Research (CAWCR) Technical Report No. 014

Grilli ST, Harris JC, Shi F, et al (2012) Numerical modeling of coastal tsunami impact dissipation and impact. Coast Eng Proc 1:1–12

Grilli ST, O'Reilly C, Harris JC, et al (2015) Modeling of SMF tsunami hazard along the upper US East Coast: detailed impact around Ocean City, MD. Nat Hazards 76:705–746. https://doi.org/10.1007/s11069-014-1522-8

Grindlay N (1998) Volume and Density Approximations of Material Involved in a Debris Avalanche on the South Slope of the Puerto Rico Trench: A Report to the Puerto Rico Civil Defense and the University of Puerto Rico Sea Grant College Program. Univ North Carolina Wilmingt

Haflidason H, Lien R, Sejrup HP, et al (2005) The dating and morphometry of the Storegga Slide. Mar Pet Geol 22:123–136. https://doi.org/10.1016/j.marpetgeo.2004.10.008

Hampton MA, Lee HJ, Locat J (1996) Submarine landslides. Rev Geophys 34:33–59. https://doi.org/10.1029/95RG03287

Harbitz CB, Løvholt F, Bungum H (2014) Submarine landslide tsunamis: How extreme and how likely? Nat Hazards 72:1341–1374. https://doi.org/10.1007/s11069-013-0681-3

Harders R, Ranero CR, Weinrebe W, Behrmann JH (2011) Submarine slope failures along the convergent continental margin of the Middle America Trench. Geochemistry, Geophys Geosystems 12:n/a-n/a. https://doi.org/10.1029/2010GC003401

Harris DL, Rovere A, Casella E, et al (2018) Coral reef structural complexity provides important coastal protection from waves under rising sea levels. Sci Adv 4:eaao4350. https://doi.org/10.1126/sciadv.aao4350

Hengesh J V, Dirstein JK, Stanley AJ (2013) Landslide geomorphology along the Exmouth plateau continental margin, North West Shelf, Australia. Aust Geomech 48:71–92

Henrich R, Hanebuth TJJ, Krastel S, et al (2008) Architecture and sediment dynamics of the Mauritania Slide Complex. Mar Pet Geol 25:17–33. https://doi.org/10.1016/j.marpetgeo.2007.05.008

Hieke W, Werner F (2000) The Augias megaturbidite in the central Ionian Sea (central Mediterranean) and its relation to the Holocene Santorini event. Sediment Geol 135:205–218. https://doi.org/10.1016/S0037-0738(00)00072-5

Hine AC, Locker SD, Tedesco LP, et al (1992) Megabreccia shedding from modern, low-relief carbonate platforms, Nicaraguan Rise. GSA Bull 104:928–943. https://doi.org/10.1130/0016-7606(1992)104<0928:MSFMLR>2.3.CO;2

Hinestrosa G, Webster JM, Beaman RJ (2016) Postglacial sediment deposition along a mixed carbonate-siliciclastic margin: New constraints from the drowned shelf-edge reefs of the Great Barrier Reef, Australia. Palaeogeogr Palaeoclimatol Palaeoecol 446:168–185. https://doi.org/10.1016/j.palaeo.2016.01.023

Hjelstuen BO, Eldholm O, Faleide JI (2007) Recurrent Pleistocene mega-failures on the SW Barents Sea margin. Earth Planet Sci Lett 258:605–618. https://doi.org/10.1016/j.epsl.2007.04.025

Holcomb RT, Searle RC (1991) Large landslides from oceanic volcanoes. Mar Georesources Geotechnol 10:19–32. https://doi.org/10.1080/10641199109379880

Holmes R, Long D, Dodd LR (1998) Large-scale debrites and submarine landslides on the Barra Fan, west of Britain. Geol Soc London, Spec Publ 129:67–79. https://doi.org/10.1144/GSL.SP.1998.129.01.05

Hopley D, Smithers SG, Parnell K (2007) The geomorphology of the Great Barrier Reef: development, diversity and change. Cambridge University Press, Cambridge

Horozal S, Bahk JJ, Lee SH, et al (2016) Late Neogene–Quaternary submarine mass wasting along the margins of the Ulleung Basin, East Sea: Geomorphologic controls and geohazard potential. Quat Int 392:69–98. https://doi.org/10.1016/j.quaint.2015.06.056

Horrillo J, Wood A, Kim G, Parambath A (2013) A simplified 3-D Navier-Stokes numerical model for landslide-tsunami: Application to the Gulf of Mexico. J Geophys Res Ocean 118:6934–6950. https://doi.org/10.1002/2012JC008689

Hubble T, Webster J, Yu P, et al (2016) Submarine Landslides and Incised Canyons of the Southeast Queensland Continental Margin. In: Lamarche G, Mountjoy J, Bull S, et al. (eds) Submarine Mass Movements and their Consequences: 7th International Symposium. Springer International Publishing, Cham, pp 125–134

Hughes TP, Kerry JT, Baird AH, et al (2018) Global warming transforms coral reef assemblages. Nature 556:492–496. https://doi.org/10.1038/s41586-018-0041-2

Hühnerbach V, Masson DG, Bohrmann G, et al (2005) Deformation and submarine landsliding caused by seamount subduction beneath the Costa Rica continental margin — new insights from high-resolution sidescan sonar data. Geol Soc London, Spec Publ 244:195–205. https://doi.org/10.1144/GSL.SP.2005.244.01.12

Hunt JE, Wynn RB, Talling PJ, Masson DG (2013) Frequency and timing of landslide-triggered turbidity currents within the Agadir Basin, offshore NW Africa: Are there associations with climate change, sea level change and slope sedimentation rates? Mar Geol 346:274–291. https://doi.org/10.1016/j.margeo.2013.09.004

Hunt JE (2012) Determining the provenance, recurrence, magnitudes and failure mechanisms of submarine landslides from the Moroccan margin and Canary Islands using distal turbidite records. University of Southampton

Iacono C Lo, Gràcia E, Zaniboni F, et al (2012) Large, deepwater slope failures: implications for landslide-generated tsunamis. Geology 40:931–934. https://doi.org/10.1130/G33446.1

Kazolea M, Filippini A, Ricchiuto M, et al (2019) Wave propagation, breaking, and overtopping on a 2D reef: A comparative evaluation of numerical codes for tsunami modelling. Eur J Mech - B/Fluids 73:122–131. https://doi.org/10.1016/j.euromechflu.2017.10.010

Kim D-H, Lynett PJ, Socolofsky SA (2009) A depth-integrated model for weakly dispersive, turbulent, and rotational fluid flows. Ocean Model 27:198–214. https://doi.org/10.1016/j.ocemod.2009.01.005

Koshimura S, Namegaya Y, Yanagisawa H (2009) Tsunami fragility: A new measure to identify tsunami damage. J Disaster Res 4:479–488. https://doi.org/10.20965/jdr.2009.p0479

Kowalik Z, Knight W, Logan T, Whitmore P (2005) Numerical modeling of the global tsunami: Indonesian tsunami of 26 December 2004. Sci Tsunami Hazards 23:40–56

Krastel S, Wynn RB, Georgiopoulou A, et al (2012) Large-Scale Mass Wasting on the Northwest African Continental Margin: Some General Implications for Mass Wasting on Passive Continental Margins. In: Yamada Y, Kawamura K, Ikehara K, et al. (eds) Submarine Mass Movements and Their Consequences. Springer Netherlands, Dordrecht, pp 189–199

Kunkel CM, Hallberg RW, Oppenheimer M (2006) Coral reefs reduce tsunami impact in model simulations. Geophys Res Lett 33:L23612. https://doi.org/10.1029/2006GL027892

Kvalstad TJ, Gauer P, Kayina AM, et al (2002) Slope stability at Ormen Lange: Offshore site investigation and geotechnics. In: Diversity and Sustainability, Proceedings of an International Conference, London. pp 233 –250

Laberg JS, Kawamura K, Amundsen H, et al (2014) A submarine landslide complex affecting the Jan Mayen Ridge, Norwegian–Greenland Sea: slide-scar morphology and processes of sediment evacuation. Geo-Marine Lett 34:51–58

Lallemand S, Lehu R, Rétif F, et al (2015) A ∼3000 years-old sequence of extreme events revealed by marine and shore deposits east of Taiwan. Tectonophysics 692:325–341. https://doi.org/10.1016/j.tecto.2015.11.001

Lamarche G, Joanne C, Collot J (2008) Successive, large mass-transport deposits in the south Kermadec fore-arc basin, New Zealand: The Matakaoa Submarine Instability Complex. Geochemistry, Geophys Geosystems 9:. https://doi.org/10.1029/2007GC001843

Lastras G, Canals M, Urgeles R, et al (2007) A walk down the Cap de Creus canyon, Northwestern Mediterranean Sea: Recent processes inferred from morphology and sediment bedforms. Mar Geol 246:176–192. https://doi.org/10.1016/j.margeo.2007.09.002

Lastras G, De Blasio FV, Canals M, Elverhøi A (2005) Conceptual and numerical modeling of the BIG'95 debris flow, western Mediterranean Sea. J Sediment Res 75:784–797. https://doi.org/10.2110/jsr.2005.063

Le Friant A, Ishizuka O, Boudon G, et al (2015) Submarine record of volcanic island construction and collapse in the Lesser Antilles arc: First scientific drilling of submarine volcanic island landslides by IODPExpedition 340. Geochemistry, Geophys Geosystems 16:420–442. https://doi.org/10.1002/2014GC005652

Lebas E, Le Friant A, Boudon G, et al (2011) Multiple widespread landslides during the long-term evolution of a volcanic island: Insights from high-resolution seismic data, Montserrat, Lesser Antilles. Geochemistry, Geophys Geosystems 12:Q05006. https://doi.org/10.1029/2010GC003451

Lebreiro SM, McCave IN, Weaver PPE (1997) Late Quaternary turbidite emplacement on the Horseshoe abyssal plain (Iberian margin). J Sediment Res Sect A Sediment Petrol Process 67:856–870

Lee C, Nott JA, Keller FB, Parrish AR (2004) Seismic expression of the Cenozoic mass transport complexes, deepwater Tarfaya-Agadir Basin, offshore Morocco. In: Offshore Technology Conference. Offshore Technology Conference, Houston, Texas, p OTC-16741-MS

Lee HJ, Normark WR, Fisher MA, et al (2004) Timing and extent of submarine landslides in Southern California. In: Offshore Technology Conference. Offshore Technology Conference, Houston, Texas, p OTC-16744-MS

Lee HJ (2009) Timing of occurrence of large submarine landslides on the Atlantic Ocean margin. Mar Geol 264:53–64. https://doi.org/10.1016/j.margeo.2008.09.009

Leslie SC, Mann P (2016) Giant submarine landslides on the Colombian margin and tsunami risk in the Caribbean Sea. Earth Planet Sci Lett 449:382–394. https://doi.org/10.1016/j.epsl.2016.05.040

Li L, Switzer AD, Wang Y, et al (2015) What caused the mysterious eighteenth century tsunami that struck the southwest Taiwan coast? Geophys Res Lett 42:8498–8506. https://doi.org/10.1002/2015GL065567

Li L, Switzer AD, Wang Y, et al (2018) A modest 0.5-m rise in sea level will double the tsunami hazard in Macau. Sci Adv 4:eaat1180. https://doi.org/10.1126/sciadv.aat1180

Lindberg B, Laberg JS, Vorren TO (2004) The Nyk Slide—morphology, progression, and age of a partly buried submarine slide offshore northern Norway. Mar Geol 213:277–289. https://doi.org/10.1016/j.margeo.2004.10.010

Liu PLF, Lynett P, Fernando H, et al (2005) Observations by the International Tsunami Survey Team in Sri Lanka. Science 308:1595. https://doi.org/10.1126/science.1110730

Locat J, Brink US ten, Chaytor JD (2010) The Block Composite Submarine Landslide, Southern New England Slope, U.S.A.: A Morphological Analysis. In: Mosher DC, Shipp RC, Moscardelli L, et al. (eds) Submarine Mass Movements and Their Consequences. Springer Netherlands, Dordrecht, pp 267–277

Locat J, Lee H, Uri S, et al (2009) Geomorphology, stability and mobility of the Currituck slide. Mar Geol 264:28–40. https://doi.org/10.1016/j.margeo.2008.12.005

Longpré M-A, Chadwick JP, Wijbrans J, Iping R (2011) Age of the El Golfo debris avalanche, El Hierro (Canary Islands): New constraints from laser and furnace 40Ar/39Ar dating. J Volcanol Geotherm Res 203:76–80. https://doi.org/10.1016/j.jvolgeores.2011.04.002

Lowe RJ, Shavit U, Falter JL, et al (2008) Modeling flow in coral communities with and without waves: A synthesis of porous media and canopy flow approaches. Limnol Oceanogr 53:1595. https://doi.org/10.4319/lo.2008.53.6.2668

Ma G, Kirby JT, Shi F (2013) Numerical simulation of tsunami waves generated by deformable submarine landslides. Ocean Model 69:146–165. https://doi.org/10.1016/j.ocemod.2013.07.001

Madin JS, Connolly SR (2006) Ecological consequences of major hydrodynamic disturbances on coral reefs. Nature 444:477–480. https://doi.org/10.1038/nature05328

Maslin M, Vilela C, Mikkelsen N, Grootes P (2005) Causes of catastrophic sediment failures of the Amazon Fan. Quat Sci Rev 24:2180–2193. https://doi.org/10.1016/j.quascirev.2005.01.016

Masson DG, Watts AB, Gee MJR, et al (2002) Slope failures on the flanks of the western Canary Islands. Earth-Science Rev 57:1–35. https://doi.org/10.1016/S0012-8252(01)00069-1

Masson DG, Harbitz CB, Wynn RB, et al (2006) Submarine landslides: processes, triggers and hazard prediction. Philos Trans R Soc London A Math Phys Eng Sci 364:2009–2039. https://doi.org/10.1098/rsta.2006.1810

McAdoo BG, Ah-Leong JS, Bell L, et al (2011) Coral reefs as buffers during the 2009 South Pacific tsunami, Upolu Island, Samoa. Earth-Science Rev 107:147–155. https://doi.org/10.1016/j.earscirev.2010.11.005

McAdoo BG, Moore A, Baumwoll J (2009) Indigenous knowledge and the near field population response during the 2007 Solomon Islands tsunami. Nat Hazards 48:73–82. https://doi.org/10.1007/s11069-008-9249-z

McAdoo BG, Pratson LF, Orange DL (2000) Submarine landslide geomorphology, US continental slope. Mar Geol 169:103–136. https://doi.org/10.1016/S0025-3227(00)00050-5

McGregor BA, Rothwell RG, Kenyon NH, Twichell DC (1993) Salt tectonics and slope failure in an area of salt domes in the northwestern Gulf of Mexico. In: Submarine landslides: selected studies in the US Exclusive Economic Zone. US Geological Survey Bulletin, pp 92–96

McMurtry GM, Watts P, Fryer GJ, et al (2004) Giant landslides, mega-tsunamis, and paleo-sea level in the Hawaiian Islands. Mar Geol 203:219–233. https://doi.org/10.1016/S0025-3227(03)00306-2

Meyer M, Geersen J, Krastel S, et al (2012) Dakar Slide Offshore Senegal, NW-Africa: Interaction of Stacked Giant Mass Wasting Events and Canyon Evolution. In: Yamada Y, Kawamura K, Ikehara K, et al. (eds) Submarine Mass Movements and Their Consequences. Springer Netherlands, Dordrecht, pp 177–188

Monismith SG, Herdman LMM, Ahmerkamp S, Hench JL (2013) Wave transformation and wave-driven flow across a steep coral reef. J Phys Oceanogr 43:1356–1379. https://doi.org/10.1175/JPO-D-12-0164.1

Moore DG, Curray JR, Emmel FJ (1976) Large submarine slide (olistostrome) associated with Sunda Arc subduction zone, northeast Indian Ocean. Mar Geol 21:211–226. https://doi.org/10.1016/0025-3227(76)90060-8

Moore GF, Strasser M (2016) Large Mass Transport Deposits in Kumano Basin, Nankai Trough, Japan. In: Lamarche G, Mountjoy J, Bull S, et al. (eds) Submarine Mass Movements and their Consequences: 7th International Symposium. Springer International Publishing, Cham, pp 371–379

Moore JG, Clague DA, Holcomb RT, et al (1989) Prodigious submarine landslides on the Hawaiian Ridge. J Geophys Res Solid Earth 94:17465–17484. https://doi.org/10.1029/JB094iB12p17465

Moore JG, Clague DA (2002) Mapping the Nuuanu and Wailau landslides in Hawaii. Hawaiian Volcanoes Deep Underw Perspect 128:223–244. https://doi.org/10.1029/GM128p0223

Mori N, Takahashi T, Yasuda T, Yanagisawa H (2011) Survey of 2011 Tohoku earthquake tsunami inundation and run-up. Geophys Res Lett 38:6–11. https://doi.org/10.1029/2011GL049210

Moscardelli L, Wood L (2008) New classification system for mass transport complexes in offshore Trinidad. Basin Res 20:73–98. https://doi.org/10.1111/j.1365-2117.2007.00340.x

Moscardelli L, Wood L, Mann P (2006) Mass-transport complexes and associated processes in the offshore area of Trinidad and Venezuela. Am Assoc Pet Geol Bull 90:1059–1088. https://doi.org/10.1306/02210605052

Moscardelli L, Wood L (2016) Morphometry of mass-transport deposits as a predictive tool. Bull Geol Soc Am 128:47–80. https://doi.org/10.1130/B31221.1

Mosher DC, Xu Z, Shimeld J (2010) The Pliocene Shelburne Mass-Movement and Consequent Tsunami, Western Scotian Slope BT - Submarine Mass Movements and Their Consequences. In: Mosher DC, Shipp RC, Moscardelli L, et al. (eds). Springer Netherlands, Dordrecht, pp 765–775

Mountjoy JJ, McKean J, Barnes PM, Pettinga JR (2009) Terrestrial-style slow-moving earthflow kinematics in a submarine landslide complex. Mar Geol 267:114–127. https://doi.org/10.1016/j.margeo.2009.09.007

Mountjoy JJ, Micallef A (2012) Polyphase Emplacement of a 30 km3 Blocky Debris Avalanche and Its Role in Slope-Gully Development. In: Yamada Y, Kawamura K, Ikehara K, et al. (eds) Submarine Mass Movements and Their Consequences. Springer Netherlands, Dordrecht, pp 213–222

Mullins HT, Dolan J, Breen N, et al (1991) Retreat of carbonate platforms: response to tectonic processes. Geology 19:1089–1092. https://doi.org/10.1130/0091-7613(1991)019<1089:ROCPRT>2.3.CO;2

Nagai R, Takabatake T, Esteban M, et al (2020) Tsunami risk hazard in Tokyo Bay: The challenge of future sea level rise. Int J Disaster Risk Reduct 45:101321. https://doi.org/https://doi.org/10.1016/j.ijdrr.2019.101321

National Geophysical Data Center / World Data Service (2020) Global Historical Tsunami Database. NOAA National Centers for Environmental Information

National Tsunami Hazard Mitigation Program (NTHMP) (2012) Proceedings and results of the 2011 NTHMP model benchmarking workshop. US Dept. of Commerce, NOAA, and NTHMP Boulder, CO

Nelson RC (1996) Hydraulic roughness of coral reef platforms. Appl Ocean Res 18:265–274. https://doi.org/10.1016/S0141-1187(97)00006-0

Newton CS, Shipp RC, Mosher DC, Wach GD (2004) Importance of mass transport complexes in the Quaternary development of the Nile Fan, Egypt. In: Offshore Technology Conference. Offshore Technology Conference, Houston, Texas

Nielsen P (1992) Coastal Bottom Boundary Layers and Sediment Transport. World Scientific, Singapore

Niemi TM, Ben-Avraham Z, Hartnady CJH, Reznikov M (2000) Post-Eocene seismic stratigraphy of the deep ocean basin adjacent to the southeast African continental margin: a record of geostrophic bottom current systems. Mar Geol 162:237–258. https://doi.org/10.1016/S0025-3227(99)00062-6

Nistor I, Palermo D, Nouri Y, et al (2009) Tsunami-Induced Forces on Structures. In: Kim YC (ed) Handbook of Coastal and Ocean Engineering. World Scientific, pp 261–286

Normark WR, Gutmacher CE (1988) Sur submarine slide, Monterey fan, central California. Sedimentology 35:629–647. https://doi.org/10.1111/j.1365-3091.1988.tb01241.x

Nott J (1997) Extremely high-energy wave deposits inside the Great Barrier Reef, Australia: Determining the cause-tsunami or tropical cyclone. Mar Geol 141:193–207. https://doi.org/10.1016/S0025-3227(97)00063-7

Nouri Y, Nistor I, Palermo DAN, Cornett A (2010) Experimental investigation of tsunami impact on free standing structures. Coast Eng J 52:43–70. https://doi.org/10.1142/S0578563410002117

Nygård A, Sejrup HP, Haflidason H, Bryn P (2005) The glacial North Sea Fan, southern Norwegian Margin: architecture and evolution from the upper continental slope to the deep-sea basin. Mar Pet Geol 22:71–84. https://doi.org/10.1016/j.marpetgeo.2004.12.001

Okada Y (1985) Surface deformation due to shear and tensile faults in a half-space. Bull Seismol Soc Am 75:1135–1154

Omira R, Ramalho I, Terrinha P, et al (2016) Deep-water seamounts, a potential source of tsunami generated by landslides? The Hirondelle Seamount, NE Atlantic. Mar Geol 379:267–280. https://doi.org/10.1016/j.margeo.2016.06.010

Omosanya KO, Alves TM (2013) A 3-dimensional seismic method to assess the provenance of mass-transport deposits (MTDs) on salt-rich continental slopes (Espirito Santo Basin, SE Brazil). Mar Pet Geol 44:223–239. https://doi.org/10.1016/j.marpetgeo.2013.02.006

Owen M, Day S, Long D, Maslin M (2010) Investigations on the Peach 4 Debrite, a Late Pleistocene Mass Movement on the Northwest British Continental Margin. In: Mosher DC, Shipp RC, Moscardelli L, et al. (eds) Submarine Mass Movements and Their Consequences. Springer Netherlands, Dordrecht, pp 301–311

Owen M, Day S, Maslin M (2007) Late Pleistocene submarine mass movements: occurrence and causes. Quat Sci Rev 26:958–978. https://doi.org/10.1016/j.quascirev.2006.12.011

Papadopoulos GA, Gràcia E, Urgeles R, et al (2014) Historical and pre-historical tsunamis in the Mediterranean and its connected seas: Geological signatures, generation mechanisms and coastal impacts. Mar Geol 354:81–109. https://doi.org/10.1016/j.margeo.2014.04.014

Piper DJW, Pirmez C, Manley PL, et al (1997) Mass-transport deposits of the Amazon Fan. In: Proceedings of the Ocean Drilling Program, Scientific Results. Ocean Drilling Program, College Station, Texas, pp 109–146

Piper DJW, Aksu AE (1987) The source and origin of the 1929 grand banks turbidity current inferred from sediment budgets. Geo-Marine Lett 7:177–182. https://doi.org/10.1007/BF02242769

Power HE, Clarke SL, Wilson O, Hubble TTCT (2015) Tsunami hazard from submarine landslides: 3D inundation modelling in New South Wales, Australia. In: Australasian Coasts & Ports Conference 2015: 22nd Australasian Coastal and Ocean Engineering Conference and the 15th Australasian Port and Harbour Conference. Engineers Australia and IPENZ, p 696

Puga-Bernabéu Á, Beaman RJ, Webster JM, et al (2016) Gloria Knolls Slide: A prominent submarine landslide complex on the Great Barrier Reef margin of north-eastern Australia. Mar Geol 385:68–83. https://doi.org/10.1016/j.margeo.2016.12.008

Puga-Bernabéu Á, Webster JM, Beaman RJ (2013a) Potential collapse of the upper slope and tsunami generation on the Great Barrier Reef margin, north-eastern Australia. Nat Hazards 66:557–575. https://doi.org/10.1007/s11069-012-0502-0

Puga-Bernabéu Á, Webster JM, Beaman RJ, et al (2019) Submarine Landslides Along the Mixed Siliciclastic-Carbonate Margin of the Great Barrier Reef (Offshore Australia). In: Submarine Landslides. American Geophysical Union, pp 313–337

Puga-Bernabéu Á, Webster JM, Beaman RJ, Guilbaud V (2011) Morphology and controls on the evolution of a mixed carbonate–siliciclastic submarine canyon system, Great Barrier Reef margin, north-eastern Australia. Mar Geol 289:100–116. https://doi.org/10.1016/j.margeo.2011.09.013

Puga-Bernabéu Á, Webster JM, Beaman RJ, Guilbaud V (2013b) Variation in canyon morphology on the Great Barrier Reef margin, north-eastern Australia: The influence of slope and barrier reefs. Geomorphology 191:35–50. https://doi.org/10.1016/j.geomorph.2013.03.001

Quataert E, Storlazzi C, van Rooijen A, et al (2015) The influence of coral reefs and climate change on wave-driven flooding of tropical coastlines. Geophys Res Lett 42:6407–6415.

https://doi.org/10.1002/2015GL064861

Ratzov G, Collot J-Y, Sosson M, Migeon S (2010) Mass-transport deposits in the northern Ecuador subduction trench: Result of frontal erosion over multiple seismic cycles. Earth Planet Sci Lett 296:89–102. https://doi.org/10.1016/j.epsl.2010.04.048

Reeder MS, Stow DA V, Rothwell RG (2002) Late Quaternary turbidite input into the east Mediterranean basin: new radiocarbon constraints on climate and sea-level control. Geol Soc London, Spec Publ 191:267–278

Rodriguez M, Chamot-Rooke N, Hébert H, et al (2013) Owen Ridge deep-water submarine landslides: implications for tsunami hazard along the Oman coast. Nat Hazards Earth Syst Sci 13:417–424. https://doi.org/10.5194/nhess-13-417-2013

Rodriguez NM, Paull CK (2000) 32. DATA REPORT: 14C dating of sediment of the uppermost Cape Fear slide plain: constraints on the timing of this massive submarine landslide. Proc Ocean Drill Program, Sci Results 164:325–332

Roeber V, Yamazaki Y, Cheung KF (2010) Resonance and impact of the 2009 Samoa tsunami around Tutuila, American Samoa. Geophys Res Lett 37:1–8. https://doi.org/10.1029/2010GL044419

Roger J, Dudon B, Krien Y, Zahibo N (2014) Discussion about tsunami interaction with fringing coral reef. In: Tsunami Events and Lessons Learned. Springer, pp 161–176

Rogers JS, Monismith SG, Koweek DA, Dunbar RB (2016) Wave dynamics of a Pacific Atoll with high frictional effects. J Geophys Res Ocean 121:350–367. https://doi.org/10.1002/2015JC011170

Rosman JH, Hench JL (2011) A framework for understanding drag parameterizations for coral reefs. J Geophys Res Ocean 116:C08025. https://doi.org/10.1029/2010JC006892

Rothwell RG, Thomson J, Kahler G (1998) Low-sea-level emplacement of a very large Late Pleistocene "megaturbidite" in the western Mediterranean Sea. Nature 392:377–380. https://doi.org/10.1038/32871

San Pedro L, Babonneau N, Gutscher M-A, Cattaneo A (2016) Origin and chronology of the Augias deposit in the Ionian Sea (Central Mediterranean Sea), based on new regional sedimentological data. Mar Geol 384:199–213. https://doi.org/10.1016/j.margeo.2016.05.005

Satake K (2007) Volcanic origin of the 1741 Oshima-Oshima tsunami in the Japan Sea. Earth, Planets Sp 59:381–390. https://doi.org/10.1186/BF03352698

Satake K, Smith JR, Shinozaki K (2002) Three-Dimensional Reconstruction and Tsunami Model of the Nuuanu and Wailau Giant Landslides, Hawaii. In: Hawaiian Volcanoes: Deep Underwater Perspectives. Washington DC American Geophysical Union Geophysical Monograph Series, pp 333–346

Sayago-Gil M, Long D, Hitchen K, et al (2010) Evidence for current-controlled morphology along the western slope of Hatton Bank (Rockall Plateau, NE Atlantic Ocean). Geo-Marine Lett 30:99–111. https://doi.org/10.1007/s00367-009-0163-5

Schambach L, Grilli ST, Kirby JT, Shi F (2018) Landslide Tsunami Hazard Along the Upper US East Coast: Effects of Slide Deformation, Bottom Friction, and Frequency Dispersion. Pure Appl Geophys 176:1–40. https://doi.org/10.1007/s00024-018-1978-7

Schnyder JSD, Eberli GP, Kirby JT, et al (2016) Tsunamis caused by submarine slope failures along western Great Bahama Bank. Sci Rep 6:1–9. https://doi.org/10.1038/srep35925

Schwab JM, Krastel S, Grün M, et al (2012) Submarine mass wasting and associated tsunami risk offshore western Thailand, Andaman Sea, Indian Ocean. Nat Hazards Earth Syst Sci 12:2609. https://doi.org/10.5194/nhess-12-2609-2012

Schwab WC, Danforth WW, Scanlon KM, Masson DG (1991) A giant submarine slope failure on the northern insular slope of Puerto Rico. Mar Geol 96:237–246. https://doi.org/10.1016/0025-3227(91)90149-X

Shao K, Liu W, Gao Y, Ning Y (2019) The influence of climate change on tsunami-like solitary wave inundation over fringing reefs. J Integr Environ Sci 16:71–88. https://doi.org/10.1080/1943815X.2019.1614071

Sheppard C, Dixon DJ, Gourlay M, et al (2005) Coral mortality increases wave energy reaching shores protected by reef flats: Examples from the Seychelles. Estuar Coast Shelf Sci 64:223–234. https://doi.org/10.1016/j.ecss.2005.02.016

Shi F, Kirby JT, Harris JC, et al (2012) A high-order adaptive time-stepping TVD solver for Boussinesq modeling of breaking waves and coastal inundation. Ocean Model 43–44:36–51. https://doi.org/10.1016/j.ocemod.2011.12.004

Shi F, Kirby JT, Tehranirad B, et al (2016) FUNWAVE-TVD fully nonlinear Boussinesq wave model with TVD solver - documentation and user‘s manual (Version 3.0). Center for Applied Coastal Research, University of Delaware. Report No.: CACR-11-03

Smith BM, Deptuck ME, Kendell KL (2010) Upper Cretaceous mass transport systems above the Wyandot Formation chalk, offshore Nova Scotia. In: Mosher DC, Shipp C, Moscardelli L, et al. (eds) Submarine Mass Movements and Their Consequences, Advances in Natural and Technological Hazards Research, Kluger-Springer Book Series. Springer, pp 605–616

Solheim A, Berg K, Forsberg CF, Bryn P (2005) The Storegga Slide complex: repetitive large scale sliding with similar cause and development. Mar Pet Geol 22:97–107. https://doi.org/10.1016/j.marpetgeo.2004.10.013

Spalding MD, Brown BE (2015) Warm-water coral reefs and climate change. Science 350:769 LP – 771. https://doi.org/10.1126/science.aad0349

Spalding MD, Ruffo S, Lacambra C, et al (2014) The role of ecosystems in coastal protection: Adapting to climate change and coastal hazards. Ocean Coast Manag 90:50–57. https://doi.org/10.1016/j.ocecoaman.2013.09.007

Storlazzi CD, Gingerich SB, van Dongeren A, et al (2018) Most atolls will be uninhabitable by the mid-21st century because of sea-level rise exacerbating wave-driven flooding. Sci Adv 4:eaap9741. https://doi.org/10.1126/sciadv.aap9741

Synolakis CE, Bardet J-P, Borrero JC, et al (2002) The slump origin of the 1998 Papua New Guinea Tsunami. Proc R Soc A Math Phys Eng Sci 458:763–789. https://doi.org/10.1098/rspa.2001.0915

Talukder AR, Völker D (2014) The Tsunami Generation Potential of Shovel and Bulli Slides in the Continental Margin SE Australia BT - Submarine Mass Movements and Their Consequences: 6th International Symposium. In: Krastel S, Behrmann J-H, Völker D, et al. (eds). Springer International Publishing, Cham, pp 539–548

Tappin DR, Watts P, Grilli ST (2008) The Papua New Guinea tsuanmi of 17 July 1998: anatomy of a catastrophic event. Nat Hazards Earth Syst Sci 8:243–266

Tappin DR, Grilli ST, Harris JC, et al (2014) Did a submarine landslide contribute to the 2011 Tohoku tsunami? Mar Geol 357:344–361. https://doi.org/10.1016/j.margeo.2014.09.043

Tappin DR, Matsumoto T, Watts P, et al (1999) Sediment slump likely caused 1998 Papua New Guinea tsunami. Eos Trans Am Geophys Union 80:329–340. https://doi.org/10.1029/99EO00241

Tehranirad B, Harris JC, Grilli AR, et al (2015) Far-field tsunami impact in the North Atlantic basin from large scale flank collapses of the Cumbre Vieja Volcano, La Palma. Pure Appl Geophys 172:3589–3616

Tehranirad B, Kirby JT, Ma G, Shi F (2012) Tsunami benchmark results for nonhydrostatic wave model NHWAVE (Version 1.1). Research Report No. CACR-11-02. Newark

Ten Brink US, Geist EL, Andrews BD (2006) Size distribution of submarine landslides and its implication to tsunami hazard in Puerto Rico. Geophys Res Lett 33:L11307. https://doi.org/10.1029/2006GL026125

Torelli L, Sartori R, Zitellini N (1997) The giant chaotic body in the Atlantic Ocean off Gibraltar: new results from a deep seismic reflection survey. Mar Pet Geol 14:125–134. https://doi.org/10.1016/S0264-8172(96)00060-8

Urgeles R, Lastras G, Canals M, et al (2003) The Big'95 Debris Flow and Adjacent Unfailed Sediments in the NW Mediterranean Sea: Geotechnicalsedimentological Properties, and Dating. In: Locat J, Mienert J, Boisvert L (eds) Submarine Mass Movements and Their Consequences: 1st International Symposium. Springer Netherlands, Dordrecht, pp 479–487

Urgeles R, Leynaud D, Lastras G, et al (2006) Back-analysis and failure mechanisms of a large submarine slide on the Ebro slope, NW Mediterranean. Mar Geol 226:185–206. https://doi.org/10.1016/j.margeo.2005.10.004

Urlaub M, Talling PJ, Masson DG (2013) Timing and frequency of large submarine landslides: Implications for understanding triggers and future geohazard. Quat Sci Rev 72:63–82. https://doi.org/10.1016/j.quascirev.2013.04.020

Uslu B, Titov V V., Eble M, Chamberlin CD (2010) Tsunami hazard assessment for Guam. NOAA Pacific Marine Environmental Laboratory Special Rep., National Oceanic and Atmospheric Administration, Seattle, WA, USA

Van Weering TCE, Nielsen T, Kenyon NH, et al (1998) Sediments and sedimentation at the NE Faeroe continental margin; contourites and large-scale sliding. Mar Geol 152:159–176. https://doi.org/10.1016/S0025-3227(98)00069-3

Vizcaino A, Gràcia E, Pallàs R, et al (2006) Sedimentology, physical properties and age of mass transport deposits associated with the Marques de Pombal Fault, Southwest Portuguese Margin. Nor Geol Tidsskr 86:177

Voight B, Le Friant A, Boudon G, et al (2012) Undrained Sediment Loading Key to Long-Runout Submarine Mass Movements: Evidence from the Caribbean Volcanic Arc. In: Yamada Y, Kawamura K, Ikehara K, et al. (eds) Submarine Mass Movements and Their Consequences. Springer Netherlands, Dordrecht, pp 417–428

Völker D, Geersen J, Behrmann JH, Weinrebe WR (2012) Submarine Mass Wasting Off Southern Central Chile: Distribution and Possible Mechanisms of Slope Failure at an Active Continental Margin. In: Yamada Y, Kawamura K, Ikehara K, et al. (eds) Submarine Mass Movements and Their Consequences: 5th International Symposium. Springer Netherlands, Dordrecht, pp 379–389

von Huene R, Ranero CR, Weinrebe W, Hinz K (2000) Quaternary convergent margin tectonics of Costa Rica, segmentation of the Cocos Plate, and Central American volcanism. Tectonics 19:314–334. https://doi.org/10.1029/1999TC001143

von Huene R, Bourgois J, Miller J, Pautot G (1989) A large tsunamogenic landslide and debris flow along the Peru Trench. J Geophys Res Solid Earth 94:1703–1714. https://doi.org/10.1029/JB094iB02p01703

Vorren TO, Laberg JS, Blaume F, et al (1998) The Norwegian–Greenland Sea continental margins: morphology and late Quaternary sedimentary processes and environment. Quat Sci Rev 17:273–302. https://doi.org/10.1016/S0277-3791(97)00072-3

Wang X, Mountjoy J, Power WL, et al (2016) Coupled Modelling of the Failure and Tsunami of a Submarine Debris Avalanche Offshore Central New Zealand. In: Lamarche G, Mountjoy J, Bull S, et al. (eds) Submarine Mass Movements and their Consequences: 7th International Symposium. Springer International Publishing, Cham, pp 599–606

Ward SN, Day S (2003) Ritter Island volcano—lateral collapse and the tsunami of 1888. Geophys J Int 154:891–902. https://doi.org/10.1046/j.1365-246X.2003.02016.x

Ward SN, Asphaug E (2003) Asteroid impact tsunami of 2880 March 16. Geophys J Int 153:F6–F10. https://doi.org/10.1046/j.1365-246X.2003.01944.x

Watts P, Grilli ST, Kirby JT, et al (2003) Landslide tsunami case studies using a Boussinesq model and a fully nonlinear tsunami generation model. Nat Hazards Earth Syst Sci 3:391–402. https://doi.org/10.5194/nhess-3-391-2003

Weaver PPE, Rothwell RG (1987) Sedimentation on the Madeira Abyssal Plain over the last 300 000 years. Geol Soc London, Spec Publ 31:71–86

Webster JM, Davies PJ, Beaman RJ, et al (2008) Evolution of drowned shelf edge reefs in the GBR; implications for understanding abrupt climate change, coral reef response and modern deep water benthic habitats—RV Southern Surveyor—voyage summary. Marine National Facility, Hobart, Tasmania, p 18

Webster JM, George NPJ, Beaman RJ, et al (2016) Submarine landslides on the Great Barrier Reef shelf edge and upper slope: A mechanism for generating tsunamis on the north-east Australian coast? Mar Geol 371:120–129. https://doi.org/10.1016/j.margeo.2015.11.008

Wei Y, Fritz HM, Titov V V., et al (2015) Source Models and Near-Field Impact of the 1 April 2007 Solomon Islands Tsunami. Pure Appl Geophys 172:657–682. https://doi.org/10.1007/s00024-014-1013-6

Wien K, Kölling M, Schulz HD (2007) Age models for the Cape Blanc Debris Flow and the Mauritania Slide Complex in the Atlantic Ocean off NW Africa. Quat Sci Rev 26:2558–2573. https://doi.org/10.1016/j.quascirev.2007.06.018

Wild C, Hoegh-Guldberg O, Naumann MS, et al (2011) Climate change impedes scleractinian corals as primary reef ecosystem engineers. Mar Freshw Res 62:205–215. https://doi.org/10.1071/MF10254

Williams SP, Davies TR, Barrows TT, et al (2014) Flank-Collapse on Ta'u Island, Samoan Archipelago: Timing and Hazard Implications. In: Sassa K, Canuti P, Yin Y (eds) Landslide Science for a Safer Geoenvironment. Springer International Publishing, Cham, pp 583–588

Winkelmann D, Geissler W, Schneider J, Stein R (2008) Dynamics and timing of the Hinlopen/Yermak Megaslide north of Spitsbergen, Arctic Ocean. Mar Geol 250:34–50. https://doi.org/10.1016/j.margeo.2007.11.013

Wynn RB, Talling PJ, Masson DG, et al (2010) Investigating the Timing, Processes and Deposits of One of the World's Largest Submarine Gravity Flows: The 'Bed 5 Event' Off Northwest Africa. In: Mosher DC, Shipp RC, Moscardelli L, et al. (eds) Submarine Mass Movements and Their Consequences. Springer Netherlands, Dordrecht, pp 463–474

Wynn RB, Masson DG, Stow DA, Weaver PP (2000) The Northwest African slope apron: a modern analogue for deep-water systems with complex seafloor topography. Mar Pet Geol 17:253–265. https://doi.org/10.1016/S0264-8172(99)00014-8

Xing HL, Ding RW, Yuen D (2015) Tsunami Hazards along the Eastern Australian Coast from Potential Earthquakes: Results from Numerical Simulations. Pure Appl Geophys 172:2087–2115. https://doi.org/10.1007/s00024-014-0904-x

Yao Y, Huang Z, Monismith SG, Lo EYM (2012) 1DH Boussinesq modeling of wave transformation over fringing reefs. Ocean Eng 47:30–42. https://doi.org/10.1016/j.oceaneng.2012.03.010

Yongfu S, Bolin H (2014) A potential tsunami impact assessment of submarine landslide at Baiyun Depression in Northern South China Sea. Geoenvironmental Disasters 1:7. https://doi.org/10.1186/s40677-014-0007-0

Young IR (1989) Wave transformation over coral reefs. J Geophys Res Ocean 94:9779–

9789. https://doi.org/10.1029/JC094iC07p09779

Young IR, Hardy TA (1993) Measurement and modelling of tropical cyclone waves in the Great Barrier Reef. Coral Reefs 12:85–95. https://doi.org/10.1007/BF00302108